

Magnetic flux distribution in type II superconductors with large demagnetization and a high edge barrier

V. N. Zabenkin,^{*} L. A. Aksel'rod, A. A. Vorob'ev, and G. P. Gordeev

St. Petersburg Institute of Nuclear Physics, Russian Academy of Sciences, 188350 Gatchina, Leningrad Region, Russia

S. A. Churin

Institute of Physics of Microstructures, Russian Academy of Sciences, 603600 Nizhny Novgorod, Russia

(Submitted 1 November 1999)

Pis'ma Zh. Éksp. Teor. Fiz. **70**, No. 12, 771–775 (25 December 1999)

The trapped flux distribution in thin wafers of both polycrystalline and granular superconductors having large demagnetization and edge barriers of different heights is measured by means of polarized neutrons. It is shown that the nature of the critical state in polycrystalline wafers, unlike that in a ceramic wafer, is not described by the Bean model.

© 1999 American Institute of Physics. [S0021-3640(99)00124-3]

PACS numbers: 74.80.Bj, 74.60.Ge, 75.20.-g

In situations where demagnetization effects can be ignored, the magnetic response of type II superconductors is well described by the Bean model¹ with the appropriate critical current density $J_C(B, T)$. In this geometry the flux lines are parallel, and the local current density J is governed by the gradient of the magnetic induction B , i.e., $J = |\nabla B|$. On the other hand, demagnetization effects become significant in a geometry characterized by a large demagnetization factor (e.g., thin films in a perpendicular field). For example, in situations where the thickness d of the sample is much smaller than its width W the current density is essentially determined entirely by the curvature of the flux lines. This relationship is evident at once from Maxwell's equation $(4\pi/c)\mathbf{J} = \nabla \times \mathbf{B} = \nabla B \times \mathbf{b} + B \nabla \times \mathbf{b}$, where $\mathbf{b} = \mathbf{B}/B$. The first term on the right-hand side of the equation gives the gradient of B and is proportional to $1/W$; the second term characterizes the curvature of the flux lines and is proportional to $1/d$.

The influence of demagnetization on the way in which the magnetic flux penetrates a type II superconductor has been analyzed theoretically in several papers. In the example of a superconducting strip it has been shown² how the magnetic flux profiles and the current densities for the Bean model change when demagnetization effects are taken into account. Three prominent features are discernible in this case: 1) Current flows in the entire sample (even in the part where the magnetic field has not penetrated); 2) the magnetic flux profile exhibits divergence at the edges of the sample; 3) the relation $J = |\nabla B|$ is not satisfied. However, despite all the differences in the distributions of the magnetic flux and the current density, the magnetic flux also begins to penetrate from the edges of the sample and advances toward the middle as the external field is increased.

The structure of the critical state in superconducting samples has been analyzed

theoretically,^{3,4} not only with demagnetization effects taken into account, but also with allowance for the edge barrier. It follows from this analysis that when, for example, superconducting films are placed in a magnetic field perpendicular to their plane, the critical state should be observed to have a structure that differs fundamentally from the Bean model.¹ The main distinguishing feature of this situation is that, without pinning, the magnetic flux immediately penetrates to the very middle of the film and becomes concentrated there. The distribution of the magnetic flux along the width of the sample (along the y axis) in this case is described by the equation

$$B(y) = \begin{cases} H_0 \sqrt{\frac{b^2 - 4y^2}{W^2 - 4y^2}} & \text{for } |y| < b/2, \\ 0 & \text{for } b/2 < |y| < W/2, \end{cases}$$

where H_0 is the magnitude of the applied magnetic field, and b is the width of the region occupied by vortices.

The presence of bulk pinning, on the other hand, has the effect that instead of a single region occupied by the magnetic flux, there are two such regions separated by a certain distance, which depends on the pinning force (the greater the pinning force, the greater is this distance). Both regions broaden as the external magnetic field is increased. Their outer boundaries approach the edges of the sample, and the inner boundaries approach the middle, where the two regions merge. For a large pinning force the distance between the flux-occupied regions can be of the order of the sample width. In this case the structure of the magnetic flux in the sample is essentially indistinguishable from the structure described by the Bean model.

We have attempted to compare the magnetic properties of a ceramic (granular) sample and a quasi-single-crystalline (nongranular) sample in this geometry. For the investigation we prepared prism-shaped wafers from these materials ($T_C = 92$ K). The side surfaces of the polycrystalline sample were reasonably smooth after polishing and comprised a mosaic of large single-crystalline grains with surface dimensions of the order of 0.2 cm^2 each. Their thickness was obviously much smaller than the thickness of the entire wafer, because the mosaic pattern on the surface of the opposite face was different. Also visible under a microscope, in addition to the large single-crystalline surfaces, were streaks of some kind of inclusions with colors that stood out in sharp contrast with the single-crystalline grains. We regard the object in question as a coarse polycrystalline block. Initially a wafer of thickness 1.3 mm was cut from this block. Once the flux distribution had been measured in this wafer, it was ground down to a thickness of 0.65 mm, and again the flux distribution was measured. The samples had widths of 5–7 mm and a height of 25 mm.

Information on the distribution of the magnetic flux trapped by a superconducting sample before and after application of an external magnetic field was obtained by three-dimensional neutron polarization analysis. This residual distribution exhibits the manner in which the field penetrates the sample.

We have described the measurement procedure in an earlier paper.⁵ A neutron beam was generated by slits of width 0.4 mm and height 7 mm and was directed along the x axis. After the sample had been cooled to the required temperature ($T < T_C$), a magnetic field directed along the thickness of the wafer (along the x axis) was applied and

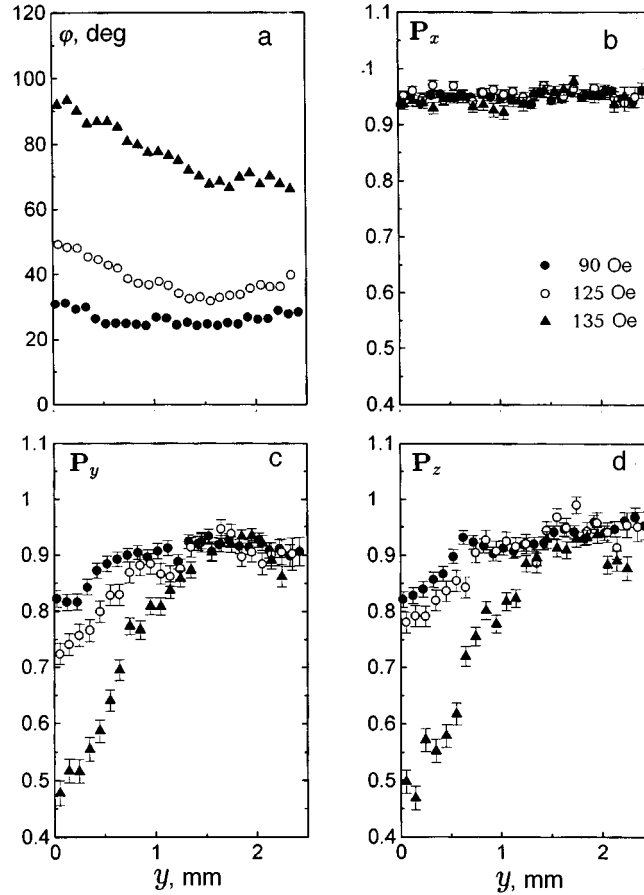


FIG. 1. Experimental results for a polycrystalline sample of thickness 1.3 mm in various applied fields at $T = 80$ K for half the sample: (a) dependence of the angle of rotation of the polarization vector on the coordinate y ; (b–d) behavior of the modulus of the polarization vector as the position of the sample is changed.

then turned off. The sample was oriented across the neutron beam (along the y axis), and the three projections of the polarization vector of the beam transmitted through the sample were measured at each site y_i of the sample for each initial polarization vector. The initial polarization vectors were directed in succession along each of the three mutually perpendicular axes (x , y , z). After the nine components of the polarization vectors had been measured, the sample was heated to $T > T_C$, and the entire procedure was repeated with a new magnitude of the external magnetic field.

The angle of rotation ϕ of the polarization vector is proportional to the magnetic induction B ($\phi = \gamma/v \cdot B \cdot L$, where L is the length of the segment of the neutron trajectory with $B \neq 0$, v is the neutron velocity, and γ is the gyromagnetic ratio of the neutron). Consequently, the magnetic flux distribution in the superconducting sample can be estimated from the dependence of the angle of rotation on the position of the sample relative to the neutron beam.

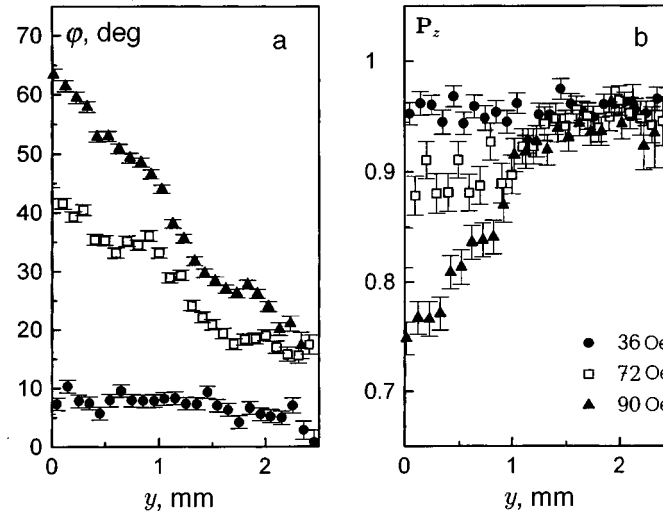


FIG. 2. Experimental results for a polycrystalline sample of thickness 0.65 mm in various applied fields at $T = 80$ K for half the sample: (a) dependence of the angle of rotation of the polarization vector on the coordinate y ; (b) behavior of the modulus of the polarization vector when the position of the sample is changed.

The experimental results are shown in Figs. 1 and 2. At $T = 80$ K the field begins to penetrate the polycrystalline sample in a field of approximately 50 Oe. As the external field is increased, the flux begins to concentrate in the middle of the sample ($y = 0$ mm), the total level increasing slightly throughout the sample (Fig. 1a).

When the polarization vector \mathbf{P}_x was initially directed along the x axis, it remained unchanged, confirming the alignment of its direction with the field (Fig. 1b). The vectors \mathbf{P}_y and \mathbf{P}_z , on the other hand, rotated through the angle ϕ . Their moduli remained constant only at the edges of the sample; in the middle, where flux concentration took place, depolarization was observed, i.e., the modulus decreased (Figs. 1c and 1d). The origin of the depolarization remains an open question. At least two causes are possible. The first is inhomogeneity of the scattered field. In all probability, however, this factor can be ruled out, because reducing the sample thickness by one half (Fig. 2) causes the depolarization to decrease, even for large sample magnetizations. The second cause is associated with the fact that the flux penetrates the sample not only along directions parallel to the y axis, but also along directions parallel to the z axis. The penetration of vortices along the z axis produces a flux distribution nonuniform in height, whose contribution to the depolarization is governed by the height of the slit (7 mm). It is important to note that if the flux distribution were described by the Bean model, the height-nonuniform flux distribution could not reach the zone irradiated by the beam. In our opinion, therefore, the depolarization of the beam is further evidence of concentration of the flux in the middle of the sample.

The distribution pattern of the trapped flux in a ceramic wafer of thickness 0.8 mm at $T = 60$ K differs from the preceding patterns and is shown in Fig. 3. Suppression of the edge barrier, as is typical of high- T_C superconductors, and strong pinning probably yield a distribution described by the Bean model. We have arrived at similar results in an

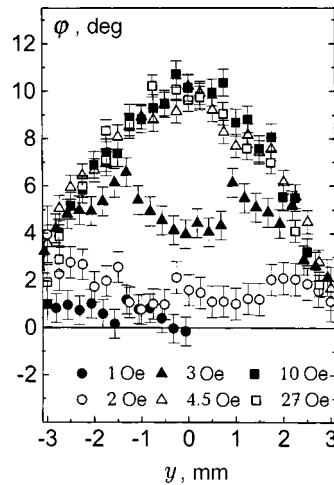


FIG. 3. Dependence of the angle of rotation of the polarization vector on the position of a ceramic sample at $T=80$ K for various applied fields.

analogous investigation of a ceramic sample in a geometry that minimized demagnetization effects,⁵ We note that the external field for which flux trapping commenced in Ref. 5 was ~ 4.5 Oe. In experiments with a thin wafer, on the other hand, the field already reaches saturation at this magnitude.

In summary, we have used neutron scattering to investigate the magnetic flux structure formed in superconductors having a large demagnetization factor and a comparatively high edge barrier. The final results corroborate the conclusion of Refs. 3 and 4 that a conceptually new structure of the critical state, manifested by concentration of the magnetic flux in the middle of the sample, occurs in superconductors having a large demagnetization factor and a sufficiently high edge barrier. The nature of these structures depends on the relation between the parameters of the edge barrier and the average bulk pinning force.

The authors are grateful to I. L. Maksimov, who inspired the setup of the reported experiments, for a discussion of their results and critical comments, along with D. Yu. Vodolazov for a discussion of the results of the study.

This work has received support from the Russian State Program "Neutron Studies of Condensed Media" and the Russian Fund for Fundamental Research (Grant No. 96-15-96775).

*¹e-mail: zabenkin@pnpi.spb.ru

¹C. P. Bean, Phys. Rev. Lett. **8**, 250 (1962).

²E. Zeldov, J. R. Clem, M. McElfresh *et al.*, Phys. Rev. B **49**, 9802 (1994).

³E. Zeldov, A. I. Larkin, V. B. Geshkenbein *et al.*, Phys. Rev. Lett. **73**, 1428 (1994).

⁴I. L. Maksimov and A. A. Elistratov, JETP Lett. **61**, 208 (1995).

⁵L. A. Akselrod, G. P. Gordeev, V. N. Zabenkin *et al.*, Physica B **221**, 219 (1994).

Monopole, half-quantum vortex, and nexus in chiral superfluids and superconductors

G. E. Volovik

Helsinki University of Technology, Low Temperature Laboratory, FIN-02015 HUT, Finland; Landau Institute of Theoretical Physics, Russian Academy of Sciences, 117334 Moscow, Russia

(Submitted 23 November 1999)

Pis'ma Zh. Éksp. Teor. Fiz. **70**, No. 12, 776–779 (25 December 1999)

Two exotic objects are still not identified experimentally in chiral superfluids and superconductors. These are the half-quantum vortex, which plays the part of the Alice string in relativistic theories [A. S. Schwarz, Nucl. Phys. B **208**, 141 (1982)], and the hedgehog in the $\hat{\mathbf{I}}$ field, which is the counterpart of the Dirac magnetic monopole. These two objects of different dimensionality are topologically connected. They form a combined object which is called a nexus [John M. Cornwall, hep-th/9911125; Phys. Rev. D **59**, 125015 (1999); Phys. Rev. D **58**, 105028 (1998)] or center monopole [N. N. Chernodub, M. I. Polikarpov, A. I. Veselov and M. A. Zubkov, Nucl. Phys. Proc. Suppl. **73**, 575 (1999)] in relativistic theories. Such a combination will permit the observation of half-quantum vortices and monopoles in several realistic geometries. © 1999 American Institute of Physics.

[S0021-3640(99)00224-8]

PACS numbers: 67.55.Fa, 74.20.-z

In relativistic quantum fields a nexus is a monopole in which N vortices of the group Z_N meet at a center (nexus) provided that the total flux of vortices adds to zero (mod N).²⁻⁴ In a chiral superfluid with an order parameter of the $^3\text{He-A}$ type, the analog of the nexus is the hedgehog in the $\hat{\mathbf{I}}$ field, in which 4 vortices meet, each with the circulation quantum number $N=1/2$. The total topological charge of the four vortices is $N=2$, which is equivalent to $N=0$ because the homotopy group, which describes the $^3\text{He-A}$ vortices, is $\pi_1=Z_4$ (Ref. 5), and thus $N=0 \pmod{2}$. Each $N=1/2$ vortex plays the part of a 1/4 fraction of the “Dirac string” terminating on the hedgehog, while the hedgehog in the $\hat{\mathbf{I}}$ field plays the part of the Dirac magnetic monopole: The distribution of the vector potential of the electromagnetic field \mathbf{A} in the vicinity of the hedgehog in the electrically charged version of $^3\text{He-A}$ (the chiral p -wave superconductor) is similar to that in the vicinity of a magnetic monopole (see, e.g., Refs. 6–8).

The order parameter describing the vacuum manifold in a chiral p -wave superfluid/superconductor ($^3\text{He-A}$ and also possibly the layered superconductor Sr_2RuO_4)⁹ is

$$A_{ai} = \Delta \hat{d}_a (\hat{e}_i^{(1)} + i \hat{e}_i^{(2)}). \quad (1)$$

Here $\hat{\mathbf{d}}$ is the unit vector of the spin-space anisotropy; $\hat{\mathbf{e}}^{(1)}$ and $\hat{\mathbf{e}}^{(2)}$ are mutually orthogonal unit vectors in the orbital space; they determine the superfluid velocity of the chiral condensate $\mathbf{v}_s = (\hbar/2m)\hat{e}_i^{(1)}\nabla\hat{e}_i^{(2)}$, where $2m$ is the mass of the Cooper pair; the orbital momentum vector is $\hat{\mathbf{I}} = \hat{\mathbf{e}}^{(1)} \times \hat{\mathbf{e}}^{(2)}$. The half-quantum vortex results from the identification of the points $\hat{\mathbf{d}}$, $\hat{\mathbf{e}}^{(1)} + i\hat{\mathbf{e}}^{(2)}$ and $-\hat{\mathbf{d}}$, $-(\hat{\mathbf{e}}^{(1)} + i\hat{\mathbf{e}}^{(2)})$, which correspond to the same order parameter, Eq. (1). It is a combination of the π vortex and π disclination in the $\hat{\mathbf{d}}$ field:

$$\hat{\mathbf{d}} = \hat{\mathbf{x}} \cos \frac{\phi}{2} + \hat{\mathbf{y}} \sin \frac{\phi}{2}, \quad \hat{\mathbf{e}}^{(1)} + i\hat{\mathbf{e}}^{(2)} = e^{i\phi/2}(\hat{\mathbf{x}} + i\hat{\mathbf{y}}), \quad (2)$$

where ϕ is the azimuthal angle around the string.

The hedgehog in the orbital momentum field, $\hat{\mathbf{I}} = \hat{\mathbf{r}}$, produces the superfluid velocity field (or the vector potential in the corresponding superconductor):

$$\mathbf{v}_s = \frac{e}{mc} \mathbf{A}, \quad \mathbf{A} = \sum_a \mathbf{A}^a, \quad (3)$$

where \mathbf{A}^a is the vector potential for the Dirac monopole with the a th Dirac string with the topological charge N_a (the number of quanta of circulation). Choosing the spherical coordinate system (r, θ, ϕ) in such a way that the string a occupies the lower half axis $z < 0$, the vector potential \mathbf{A}^a of such string can be written as:⁸

$$\mathbf{A}^a = \frac{\hbar c}{4e r} N_a \hat{\phi} \frac{1 - \cos \theta}{\sin \theta}. \quad (4)$$

The superfluid vorticity and the corresponding magnetic field in superconductor are

$$\nabla \times \mathbf{v}_s = -\frac{\hbar}{4m} \frac{\mathbf{r}}{r^3} \sum_a N_a + \frac{h}{2m} \sum_a N_a \int_0^R dr \delta(\mathbf{r} - \mathbf{r}_a(r)), \quad (5)$$

$$\mathbf{B} = -\frac{\hbar c}{4e} \frac{\mathbf{r}}{r^3} \sum_a N_a + \frac{hc}{2e} \sum_a N_a \int_0^R dr \delta(\mathbf{r} - \mathbf{r}_a(r)), \quad \sum_a N_a = -2. \quad (6)$$

Here $\mathbf{r}_a(r)$ is the position of the a th line, assuming that the lines are emanating radially from the monopole, i.e., the coordinate along the line is the radial coordinate. The regular part of the magnetic field corresponds to a monopole with magnetic charge $g = \hbar c/2e$; the magnetic flux $4\pi g$ of the monopole is supplied by the Abrikosov vortices. The lowest energy of the monopole occurs when all the vortices emanating from the monopole have the lowest circulation number: this means that there must be four vortices with $N_1 = N_2 = N_3 = N_4 = -1/2$.

The half-quantum vortices are accompanied by spin disclinations. Assuming that the $\hat{\mathbf{d}}$ field is confined in the plane, one can characterize the disclinations by the winding numbers ν_a , which have values $\pm 1/2$ in half-quantum vortices. The corresponding spin-superfluid velocity \mathbf{v}_{sp} is

$$\mathbf{v}_{sp} = \frac{e}{mc} \sum_{a=1}^4 \nu_a \mathbf{A}^a, \quad \sum_{a=1}^4 \nu_a = 0, \quad (7)$$

where the last condition means the absence of the monopole in the spin sector of the order parameter. Thus we have $\nu_1 = \nu_2 = -\nu_3 = -\nu_4 = 1/2$.

The spin-orbit coupling can be neglected if the size of the bubble is less than spin-orbit length (about $10 \mu\text{m}$ in $^3\text{He-A}$). If it is assumed that the superfluid velocity is everywhere perpendicular to $\hat{\mathbf{I}}$ and has the form $\mathbf{v}_s = \tilde{\mathbf{v}}_s(\theta, \phi)/r$, the energy of the nexus in the spherical bubble of radius R is

$$\begin{aligned}
 E &= \int_0^R r^2 dr \int d\Omega \left(\frac{1}{2} \rho_s \mathbf{v}_s^2 + \frac{1}{2} \rho_{\text{sp}} \mathbf{v}_{\text{sp}}^2 \right) = R \int d\Omega \left(\frac{1}{2} \rho_s \tilde{\mathbf{v}}_s^2 + \frac{1}{2} \rho_{\text{sp}} \tilde{\mathbf{v}}_{\text{sp}}^2 \right) \\
 &= \frac{1}{2} R \int d\Omega ((\rho_s + \rho_{\text{sp}})[(\tilde{\mathbf{A}}^1 + \tilde{\mathbf{A}}^2)^2 + (\tilde{\mathbf{A}}^3 + \tilde{\mathbf{A}}^4)^2] \\
 &\quad + 2(\rho_s - \rho_{\text{sp}})(\tilde{\mathbf{A}}^1 + \tilde{\mathbf{A}}^2)(\tilde{\mathbf{A}}^3 + \tilde{\mathbf{A}}^4)), \\
 \tilde{\mathbf{A}}^a(\theta, \phi) &= \frac{mcr}{e} \mathbf{A}^a. \tag{8}
 \end{aligned}$$

In the simplest case, which occurs in the ideal Fermi gas approximation, when the Fermi liquid corrections are neglected, one has $\rho_s = \rho_{\text{sp}}$.¹⁰ In this case the $1/2$ vortices with positive spin current circulation ν do not interact with $1/2$ vortices with negative ν . The energy minimum occurs when the orientations of two positive- ν vortices are opposite, so that these two $1/4$ fractions of the Dirac strings form one line along the diameter (see Fig. 1). The same happens for the other fractions with negative ν . The mutual orientations of the two diameters is arbitrary in this limit. However, in real $^3\text{He-A}$ one has $\rho_{\text{sp}} < \rho_s$ (Ref. 10). If ρ_{sp} is slightly smaller than ρ_s , the positive- ν and negative- ν strings repel each other, so that the equilibrium angle between them is $\pi/2$. In the extreme case $\rho_{\text{sp}} \ll \rho_s$, the ends of four half-quantum vortices form the vertices of a regular tetrahedron.

Such monopole can be experimentally realized in the mixed $^4\text{He}/^3\text{He}$ droplets obtained by the nozzle beam expansion of He gases.¹¹ The ^4He component of the mixture forms the cluster in a central region of the droplet.¹¹ If the size of the cluster is comparable with the size of the droplet, the radial distribution of the $\hat{\mathbf{I}}$ vector is stabilized by the boundary conditions on the surface of the droplet and on the boundary of the cluster (see Fig. 1). The ^4He cluster plays the part of the core of the nexus. The half-quantum vortices emanating from the nexus are well defined if the radius of the droplet exceeds the coherence length $\xi \sim 200\text{--}500 \text{ \AA}$.

In a p -wave superconductor such a monopole will be formed in a thin spherical layer. In Sr_2RuO_4 superconductor the spin-orbit coupling between the spin vector $\hat{\mathbf{d}}$ and crystal lattice seems to align the $\hat{\mathbf{d}}$ vector along $\hat{\mathbf{I}}$ (Ref. 12). In this case the half-quantum vortices are energetically unfavorable, and instead of 4 half-quantum vortices one would have 2 singly quantized vortices in the spherical shell.

A monopole of this kind can also be formed in the so-called ferromagnetic Bose condensate in optical traps. Such a condensate is described by a vector or spinor chiral order parameter.¹³

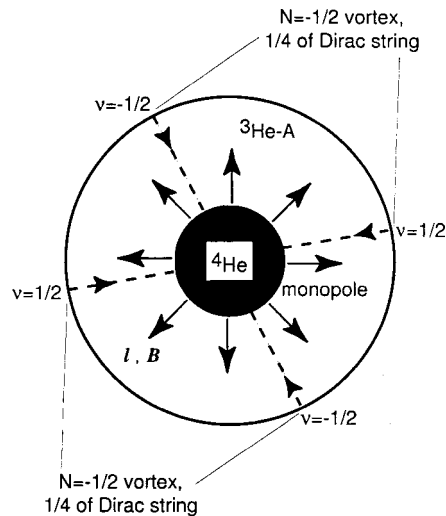


FIG. 1. The outward-pointing arrows show the distribution of the orbital momentum $\hat{\mathbf{I}}$ field and simultaneously the distribution of superfluid vorticity $\nabla \times \mathbf{v}$, in superfluid ${}^3\text{He-A}$ or of the magnetic field \mathbf{B} in a chiral superconductor. The inward-pointing arrows show the direction of the vorticity or magnetic flux concentrated in 4 half-quantum vortices (dashed lines). The charge $\nu = \pm 1/2$ is the number of quanta of circulation of the spin current velocity \mathbf{v}_{sp} . The stability of the monopole at the center of the droplet is supported by the cluster of the ${}^4\text{He}$ liquid, which provides the radial boundary condition for the $\hat{\mathbf{I}}$ vector. The cluster forms the core of the monopole.

There are interesting properties of the system related to the fermionic spectrum of such objects. In particular, the number of fermion zero modes on the $N = 1/2$ vortex under discussion is smaller by a factor of two than that on the vortex with $N = 1$. This is because this $N = 1/2$ vortex can be represented as the $N = 1$ vortex in one spin component with no vortices in another spin component. Thus, according to Ref. 14, in the core of the $N = 1/2$ vortex there is one fermionic level (per 2D layer) with exactly zero energy. Since the zero-energy level can be either filled or empty, there is an entropy $(1/2)\ln 2$ per layer related to the vortex. The factor $(1/2)$ appears because the particle excitation coincides with the antiparticle (hole) excitation in superconductors, i.e., the quasiparticle is a Majorana fermion; see also Ref. 15. Such a fractional entropy also arises in the Kondo problem.¹⁶ According to Ref. 17, the $N = 1$ vortex has spin $S = 1/4$ per layer, and this implies a spin $S = 1/8$ per layer for the $N = 1/2$ vortex. Similarly the anomalous fractional charge of the $N = 1/2$ vortex is $1/2$ of that discussed for the $N = 1$ vortex.¹⁸

I thank M. Feigel'man and D. Ivanov for discussions. This work was supported in part by the Russian Fund for Fundamental Research and by the European Science Foundation.

¹A. S. Schwarz, Nucl. Phys. B **208**, 141 (1982).

²John M. Cornwall, <http://xxx.lanl.gov/abs/hep-th/9911125>; Phys. Rev. D **59**, 125015 (1999); Phys. Rev. D **58**, 105028 (1998).

³N. N. Chernodub, M. I. Polikarpov, A. I. Veselov and M. A. Zubkov, Nucl. Phys. Proc. Suppl. **73**, 575 (1999).

⁴H. Reinhardt, M. Engelhardt, K. Langfeld *et al.*, <http://xxx.lanl.gov/abs/hep-th/9911145>.

- ⁵G. E. Volovik and V. P. Mineev, JETP Lett. **24**, 561 (1976).
⁶S. Blaha, Phys. Rev. Lett. **36**, 874 (1976).
⁷G. E. Volovik and V. P. Mineev, JETP Lett. **23**, 593 (1976).
⁸G. E. Volovik, Usp. Fiz. Nauk **143**, 73 (1984) [Sov. Phys. Usp. **27**, 363 (1984)].
⁹M. Rice, Nature (London) **396**, 627 (1998); K. Ishida, H. Mukuda, Y. Kitaoka *et al.*, Nature (London) **396**, 658 (1998).
¹⁰D. Vollhardt and P. Wölfle, *The Superfluid Phases of ^3He* , Taylor & Francis, London, 1990.
¹¹S. Grebenev, M. Hartmann, A. Lindinger *et al.*, to be published in Physica B **284-288** (2000).
¹²Kwai-Kong Ng and M. Sigrist, <http://xxx.lanl.gov/abs/cond-mat/9911325>.
¹³Tin-Lun Ho, Phys. Rev. Lett. **81**, 742 (1998).
¹⁴G. E. Volovik, JETP Lett. **70**, 609 (1999).
¹⁵N. Read and D. Green, <http://xxx.lanl.gov/abs/cond-mat/9906453>.
¹⁶A. V. Rozhkov, <http://xxx.lanl.gov/abs/cond-mat/9711181>.
¹⁷D. A. Ivanov, <http://xxx.lanl.gov/abs/cond-mat/9911147>.
¹⁸J. Goryo, <http://xxx.lanl.gov/abs/cond-mat/9908113>.

Published in English in the original Russian journal. Edited by Steve Torstveit.

Observation of fine structure in the photoluminescence spectrum of an Er^{3+} ion in an amorphous silicon matrix

A. A. Andreev, V. G. Golubev,^{*} A. V. Medvedev, A. B. Pevtsov,
and N. A. Feoktistov

*A. F. Ioffe Physicotechnical Institute, Russian Academy of Sciences,
194021 St. Petersburg, Russia*

V. F. Masterov[†]

St. Petersburg State Technical University, 195251 St. Petersburg, Russia

S. B. Aldabergenova and P. C. Taylor

University of Utah, Salt Lake City, UT 84112-0830, USA

(Submitted 22 November 1999)

Pis'ma Zh. Éksp. Teor. Fiz. **70**, No. 12, 780–783 (25 December 1999)

A multicomponent Stark structure corresponding to a $4I_{13/2} \rightarrow 4I_{15/2}$ transition in the $4f^{11}$ shell of Er^{3+} ions is observed in hydrogenated amorphous silicon ($a\text{-Si:H}$) subjected to low-temperature (150 °C) anneal. The observation of narrow, strong components indicates that the erbium ions form a highly ordered local surrounding (Er–O–Si nano-clusters) in the labile, disordered structural network of $a\text{-Si:H}$.
© 1999 American Institute of Physics. [S0021-3640(99)00324-2]

PACS numbers: 78.55.Ap, 71.70.Ej

A characteristic feature of the electronic structure of rare-earth elements is strong shielding of the partially filled inner $4f$ shell with outer-shell electrons. When ions of rare-earth elements are situated in a matrix, the $4f$ shell interacts weakly with the crystal field generated by nearest-neighbor atoms. The main splitting of $4f$ states is the result of spin-orbit interaction. The crystal field merely lifts the degeneracy of the spin-orbit split levels.

The atomlike spectra of internal $f-f$ luminescence in perfect crystalline semiconductor matrices consist of series of Stark multiplets. A Stark structure is scarcely detected at all in disordered semiconductor matrices, owing to strong, nonuniform broadening of the individual components of the multiplets.

In the present study the photoluminescence spectrum in a disordered semiconductor — erbium-doped amorphous hydrogenated silicon — has been observed to have a multicomponent structure corresponding to an internal $4I_{13/2} \rightarrow 4I_{15/2}$ transition in the $4f^{11}$ shell of Er^{3+} ions. The minimum width of the Stark components at 77 K attains 2 meV. This value is consistent with the usual recorded width of the Stark components in the emission spectra of Er^{3+} centers in crystalline silicon.^{1,2} The structure is sharply en-

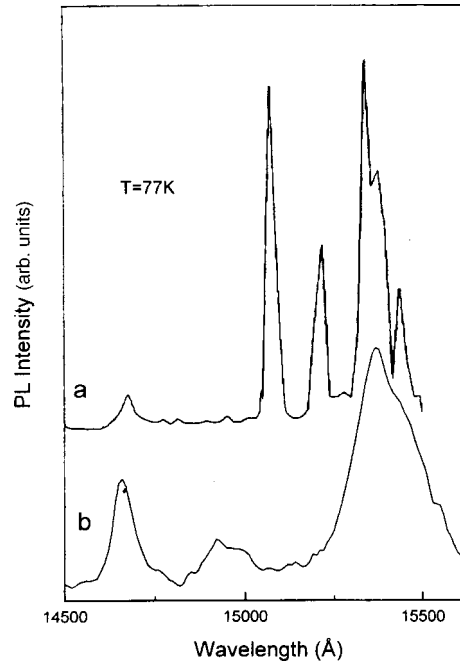


FIG. 1. Photoluminescence spectra, at $T=77$ K, of two a -Si(Er):H films subjected to low-temperature (150°C) anneal. The films were prepared by magnetron sputtering (a) and PECVD (b).

hanced by a short-term (10–20 min), low-temperature ($T < 200^\circ\text{C}$) anneal of a -Si(Er):H films.

Figure 1 shows the photoluminescence spectra of two a -Si(Er):H films thermally annealed at 150°C in a liquid nitrogen atmosphere. This anneal temperature is much lower than the temperature (400 – 500°C) at which the crystallization process is initiated in a -Si(Er):H.³ The amorphism of the structural network was monitored by Raman spectroscopy.⁴ The films were prepared by the cosputtering of a composite Si–Er target with simultaneous decomposition of the reactive gas in a magnetron discharge plasma⁵ and by plasma-enhanced chemical vapor deposition (PECVD).⁶ The deposition temperature was 200°C . The photoluminescence excitation source was an argon laser (4880 Å and 5145 Å). The photoluminescence signal was recorded by a cooled germanium photodiode.

The observation of such narrow photoluminescence lines is unequivocal evidence that the erbium ions reside in a highly ordered local surrounding. The dispersion of the lengths of the interatomic bonds and the angles between them in the nearest-neighbor local surrounding of Er^{3+} ions should not exceed the characteristic values for crystalline silicon.

Amorphous solids are known to be systems frozen in a metastable state far from the absolute energy minimum.⁷ It is possible for metastable, highly ordered local atomic configurations (nanoclusters) to form around Er^{3+} ions imbedded in a labile matrix of

amorphous silicon.⁸ The observed fine structure of the Stark levels reveals the formation of such local configurations.

We note that impurity atoms in crystalline silicon are situated at nodes or in interstices of the lattice, which are characterized by a finite number of specific local symmetries. For example, in crystalline silicon implanted with erbium (10^{19} Er/cm³) and oxygen (10^{20} O/cm³) and subjected to appropriate thermal anneals, according to extended x-ray absorption fine structure (EXAFS) data, the nearest-neighbor atoms in the erbium surrounding are 5.0 ± 0.5 oxygen ions at an average distance of 2.26 ± 0.02 Å. This configuration is very close to the surrounding of erbium in Er₂O₃ (six oxygen atoms at a distance of 2.26 Å).⁹ Also, the most probable local symmetries of sites occupied by Er³⁺ ions are T_d , C_3 , and D_{2d} (Ref. 10).

Recent EXAFS results in *a*-Si(Er):H prepared by sputtering¹¹ suggest that the nearest neighbors of an Er³⁺ ion in such an ordered nanocluster could be, for example, two or three oxygen atoms (at an average distance of 2.07–2.14 Å) and silicon atoms (3.10–3.17 Å). Consequently, in amorphous silicon under certain conditions (method of preparation, cooldown temperature, anneal temperature, etc.) the symmetry of the local surrounding of Er³⁺ ions, which generates a ligand intracrystalline field, can be lower than in crystalline silicon. The low symmetry and probably minute dimensions of the resulting Er–O–Si clusters can also significantly alter the hybridization of band and impurity states. Consequently, both the energy spectrum of the luminescence centers and the probabilities of electron transitions change in the highly localized *f*-electron system. These changes explain why the experimental photoluminescence spectra contain narrow lines having a comparable intensity, but much shorter wavelength than the wavelength (15340 Å) of the transition between the lowest sublevels of the $4I_{13/2}$ and $4I_{15/2}$ multiplets of the Er³⁺ ions in erbium-doped crystalline silicon.^{2,12,13} The recorded differences in the ratio between the intensities of the components and in the number of components of the Stark structure in *a*-Si(Er):H films prepared by different technologies (Fig. 1) suggest the possible existence of several types of low-symmetry erbium-containing centers.

Increasing the anneal temperature to 300 °C almost completely eliminated the fine structure from the photoluminescence spectra and caused the remaining lines to broaden considerably. This behavior is attributed to an increase in the efficiency of gettering of oxygen ions by erbium ions.⁹ The high efficiency of this process imparts high mobility to the impurity atoms in amorphous silicon at the given temperature.¹⁴ First of all, gettering lowers the density of the lowest-symmetry emission centers, which contain the smallest number of oxygen atoms in the nearest-neighbor surrounding of the Er³⁺ ions. As a result, transition lines having a wavelength smaller than 15340 Å vanish. The density of centers containing a large number of oxygen atoms increases accordingly. Second, gettering induces an increase in the static disorder of the as-prepared structural network of amorphous silicon near the boundaries of the ordered Er–O–Si nanoclusters, which leads to nonuniform broadening of the emission lines. Third, the process increases the intensity^{2,9} of the remaining detectable lines, making it possible to observe an essentially unstructured, strong, broad photoluminescence band at room temperature (Fig. 2).

To summarize, Er³⁺ ions in a disordered matrix of hydrogenated amorphous silicon can function as centers for the nucleation of metastable nanoclusters having a highly ordered structure. Observation of the evolution of Stark splitting of the terms of the

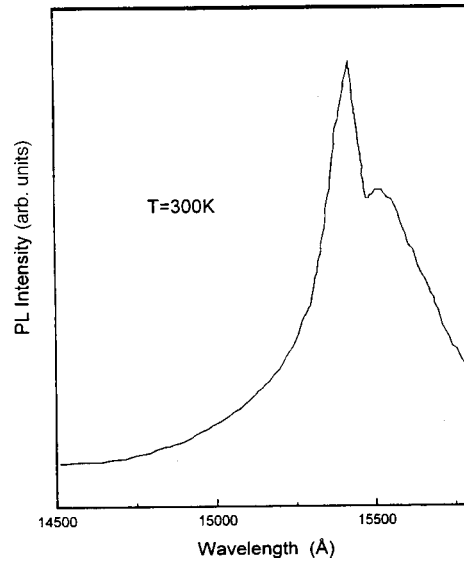


FIG. 2. Photoluminescence spectrum, at $T=300$ K, of an a -Si(Er):H film deposited by magnetron sputtering and annealed at $T=350$ °C.

highly localized f -electron system of these ions affords a sensitive investigative probe for studying the formation and destruction of such clusters.

This work has received financial support from the Russian Fund for Fundamental Research (Project No. 98-02-17350), the International Scientific-Technical Program “Physics of Solid-State Nanostructures” (Project No. 99-1107), and the United States National Academy of Sciences.

*¹e-mail: golubev@gvg.ioffe.rssi.ru

[†]Deceased.

¹H. Ennen, G. Pomrenke, A. Axmann *et al.*, Appl. Phys. Lett. **46**, 381 (1985).

²J. Michel, J. L. Benton, R. F. Ferrante *et al.*, J. Appl. Phys. **70**, 2672 (1991).

³A. B. Pevtsov, V. Yu. Davydov, N. A. Feoktistov *et al.*, Phys. Rev. B **52**, 955 (1995).

⁴V. G. Golubev, V. Yu. Davydov, A. V. Medvedev *et al.*, Fiz. Tverd. Tela (St. Petersburg) **39**, 1348 (1997) [Phys. Solid State **39**, 1197 (1997)].

⁵A. A. Andreev, V. B. Voronkov, V. G. Golubev *et al.*, Fiz. Tekh. Poluprovodn. **33**, 106 (1999) [Semiconductors **33**, 93 (1999)].

⁶V. B. Voronkov, V. G. Golubev, N. I. Gorshkov *et al.*, Fiz. Tverd. Tela (St. Petersburg) **40**, 1433 (1998) [Phys. Solid State **40**, 1301 (1998)].

⁷Yu. M. Galperin, V. G. Karpov, and V. I. Kozub, Adv. Phys. **38**, 669 (1989).

⁸G. Lucovsky and W. B. Pollard, in *The Physics of Hydrogenated Amorphous Silicon*, Vol. 2: *Electronic and Vibrational Properties*, J. D. Joannopoulos and G. Lucovsky (eds.), Springer-Verlag, Berlin-New York (1984).

⁹A. Terrasi, G. Franzo, S. Coffa *et al.*, Appl. Phys. Lett. **70**, 1712 (1997).

¹⁰D. E. Wortman, C. A. Morrison, and J. L. Bradshaw, J. Appl. Phys. **82**, 2580 (1997).

¹¹C. Piamonteze, A. C. Iniguez, L. R. Tessler *et al.*, Phys. Rev. Lett. **81**, 4652 (1998).

¹²Y. S. Tang, K. C. Heasman, W. P. Gillin *et al.*, Appl. Phys. Lett. **55**, 432 (1989).

¹³H. Przybylinska, W. Jantch, Yu. Suprunin-Belevitch *et al.*, Phys. Rev. B **54**, 2532 (1996).

¹⁴J. Kakalios, R. A. Street, and W. B. Jackson, Phys. Rev. Lett. **59**, 1037 (1987).

Photoinduced transformation of luminescence centers in C₆₀ crystals at high pressure

V. D. Negrii^{*)} and K. P. Meletov

Institute of Solid-State Physics, Russian Academy of Sciences, 142432 Chernogolovka, Moscow Region, Russia

(Submitted 22 November 1999)

Pis'ma Zh. Éksp. Teor. Fiz. **70**, No. 12, 784–788 (25 December 1999)

The influence of laser irradiation on the photoluminescence spectra of perfect C₆₀ crystals in the orientationally disordered phase is investigated. It is shown that irradiation of the crystals with low-power light for short durations at $T=200$ K produces radical changes in the luminescence spectrum. The pressure dependences of the spectral bands of the phototransformed and initial (without irradiation) spectra differ significantly, indicating a photoinduced structural transformation of the X centers responsible for the luminescence of C₆₀. The phototransformed C₆₀ crystals are stable against further exposure to light irradiation and pressure. © 1999 American Institute of Physics.
[S0021-3640(99)00424-7]

PACS numbers: 78.55.Hx, 62.50.+p, 71.35.Aa, 61.80.Ba

The low-temperature photoluminescence spectra of high-quality C₆₀ crystals are known to have a line structure attributable to the radiative recombination of Frenkel excitons localized at so-called X centers.^{1,2} A C band associated with the radiative recombination of free Frenkel excitons is also observed in crystals having a relatively low density of X centers and a low luminescence quantum efficiency.³ The properties of X centers and their relationship to the structure of the luminescence spectrum of C₆₀ crystals are of considerable interest and have been investigated in a number of papers. However, despite significant progress in research on the electronic states of C₆₀, the real nature of X centers remains elusive for the most part. Studies of the luminescence spectra of the purest C₆₀ crystals have shown that the X centers are not associated with impurities, rather they are more likely attributable to defects of the crystal structure. Regardless of the degree of structural perfection of the investigated samples, the presence of orientational defects is a characteristic attribute of fullerite. The occurrence of an orientational ordering phase transition in C₆₀ crystals at $T=260$ K and the cessation of random molecular rotation below this temperature are well known.⁴ However, the molecules execute discrete rotations between two energywise close orientational states down to 80 K, below which each molecular motion is frozen, and a phase of the orientational glass type is established.⁵

It is also known that the dimerization of molecules is observed in the orientationally disordered phase of laser-irradiated C₆₀, and polymerization of the as-grown material

takes place when the laser power is increased.⁶ Detailed studies of the optical spectra and crystal structure of C_{60} have shown that polymerization also takes place under the combined influence of pressure and high temperatures, resulting in the formation of numerous, structurally different phases.^{7,8} All these transformations are accompanied by a radical change in the initial photoluminescence spectrum.

Modification of the luminescence spectra in laser irradiation has also been observed in the orientationally ordered phase of C_{60} crystals at standard pressure and at temperatures of 5 K, 77 K and 120 K. This phenomenon was achieved by pre-irradiating local zones of the crystal with a laser beam at power densities ranging from 5 W/cm² to 50 W/cm² and then recording the photoluminescence spectra from the irradiated and control zones of the crystal at $T \sim 5$ K and an excitation power density ~ 1 W/cm². It was established that irradiation of the crystals at temperatures in the vicinity of 5 K and 77 K induces a relative variation of the intensities of the emission bands of X_2 and X_3 centers, and irradiation at 120 K is accompanied by diminution of the X_2 - and X_3 -center bands and enhancement of the intensity of the C band.⁹ Similar results on the influence of laser irradiation on the photoluminescence spectra in the low-temperature range are also reported in Ref. 10.

Consequently, the existing experimental data indicate that light has a powerful influence on the spectrum of localized electronic states of C_{60} crystals. Photoinduced processes in the orientationally ordered phase of fullerite, in particular, the low-temperature, photoinduced structural transformation of X centers, are of major interest in this regard. With the latter phenomenon in mind, in the present study we report an investigation of the combined influence of high pressure and laser irradiation on C_{60} crystals and show that a radical transformation of the photoluminescence spectra takes place in the temperature range 140–250 K. We confirm that the pressure dependence of the phototransformed and initial photoluminescence spectra differ significantly, and the phototransformed samples are stable against subsequent light irradiation and pressure. We have shown that the photoinduced structural transformation of X centers also takes place at high pressure, and when the latter is suddenly dropped to standard pressure, the photoluminescence spectra of the samples transformed at different pressures are identical.

The measurements were carried out on a large series of C_{60} crystals grown from the vapor phase. The photoluminescence spectra were recorded by means of an automated spectrometer incorporating a DFS-12 dual monochromator, a liquid nitrogen-cooled FEU-62 photomultiplier, and a 5S1 photon counting system. All the photoluminescence spectra were normalized to the calibrated spectrum of a tungsten lamp. Luminescence was excited by a helium-neon laser with its power output limited by optical filters. High-pressure measurements in liquid nitrogen or helium vapor were performed using a miniature diamond anvil cell of the Merrill–Bassett type enclosed in a helium optical thermostat. Pressure was transmitted by means of a 4:1 methanol-ethanol mixture,¹¹ and its value was determined from the position of the ruby luminescence R_1 line within ~ 0.05 -GPa error limits.¹² The measurements were performed on crystals having a mirror finish and dimensions of $100 \times 100 \times 40$ μm , which are close to the dimensions of the working volume of the high-pressure cell.

The photoinduced structural transformation was investigated over a wide range of temperatures on crystals with a relatively high photoluminescence quantum efficiency, whose spectra were dominated by the emission bands of X_3 , X_4 , and X_5 centers. They

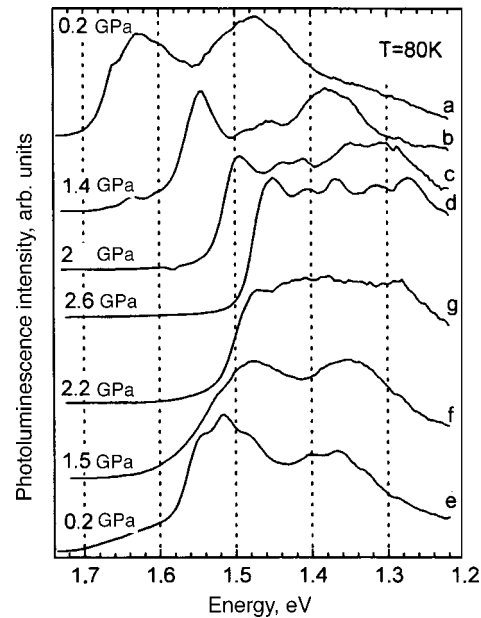


FIG. 1. Photoluminescence spectra of nonirradiated (a–d) and laser-irradiated (e–g) C_{60} crystals at a temperature $T=80$ K and pressures up to 3.0 GPa.

show that the variations of the photoluminescence spectra takes place in the temperature interval 180–240 K and are appreciable even at a very low excitation level $\cong 5 \times 10^{-3} \text{ W/cm}^2$. The temperature dependence of the phototransformation efficiency at standard pressure is bell-shaped with a maximum in the vicinity of $T \cong 200$ K. Consequently, at $T=200$ K laser irradiation of the crystal for $\cong 15$ min at a power density $\cong 0.2 \text{ W/cm}^2$ leads to radical (more than 95%) restructuring of the initial spectrum. It is important to note that direct measurements of the photoluminescence spectra were performed at $T=80$ K, i.e., at a temperature where phototransformation is frozen.

Figure 1 shows the initial (a) and phototransformed (e) photoluminescence spectra determined at a pressure ~ 0.2 GPa under the above-stated irradiation conditions. The measurements show that spectrum (e) is stable in the presence of further irradiation of the crystal over the entire temperature range up to $T=260$ K. Temperature cycling of the samples in the interval 5–300 K without irradiation by any kind of light does not produce appreciable changes in the high-temperature photoluminescence spectra. On the other hand, the irradiation of these crystals at $T=300$ K for the sample laser excitation parameters alters the low-temperature photoluminescence spectrum in connection with flare-up and pronounced broadening of the bands of the initial spectrum. Similar effects have been observed in all the C_{60} crystals at our disposal, but irradiation does not have such a pronounced influence on their photoluminescence spectra.

Figure 1 also shows the photoluminescence spectra of the as-grown and phototransformed crystals at various pressures. Spectra (a)–(d) refer to the nonirradiated crystal, and spectra (e)–(g) to a crystal preirradiated at a temperature $T=200$ K and pressure of 0.2 GPa. It is evident from Fig. 1(a–d) that, apart from an overall shift of the photolu-

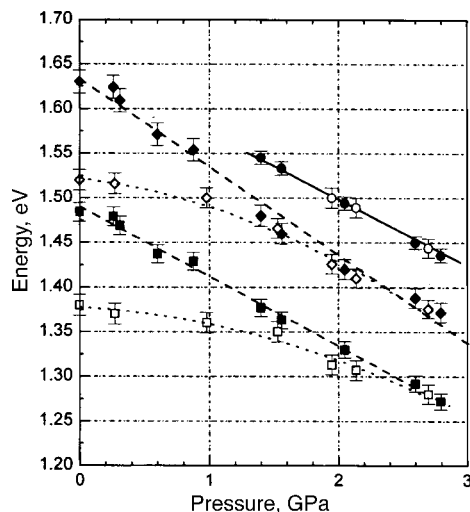


FIG. 2. Pressure dependence of the band positions in the low-temperature photoluminescence spectrum of nonirradiated (dark symbols) and irradiated (light symbols) C_{60} crystals. The dark and light dots represent the pressure dependence of the position of the C band.

minescence spectrum into the long-wavelength region, its shape also changes as the pressure is increased. At $P \geq 1.2$ GPa a band that is scarcely perceptible in the initial photoluminescence spectrum flares up in the short-wavelength region. On the other hand, fine structure becomes increasingly evident in the broad bands of the initial photoluminescence spectrum as the pressure is increased. Such changes have also been observed in the spectra of the preirradiated crystal, but are not nearly as pronounced.

Figure 2 shows the pressure dependence of the positions of the spectral bands in the photoluminescence spectra of the as-grown (dark symbols) and phototransformed (light symbols) crystals. It is evident from Fig. 2 that the pressure variations of the bands of preirradiated and nonirradiated crystals differ significantly in the low-pressure range, but then they become more alike as the pressure is increased, and at $P \geq 1.8$ GPa they essentially coincide. The difference in the pressure dependence of the photoluminescence bands of the as-grown and irradiated crystals in the initial pressure range indicates that what happens during irradiation is not merely a redistribution of the photoluminescence intensity among different luminescence centers of the as-grown crystal, but a transformation of the core structure of the crystal. At the same time, the increasing similarity of the photoluminescence spectra of the as-grown and phototransformed samples with increasing pressure suggests that the latter could be unstable under the influence of high pressure and revert to the as-grown state. It is also essential to note that pressure-enhanced band in the spectrum of the nonirradiated crystals is in the same position and exhibits the same pressure dependence as the C band, which we have previously identified with the emission of free excitons.³

We have carried out an experiment to answer the question of whether the phototransformed samples are stable and whether phototransformation takes place at high pressure; the results are shown in Fig. 3. Curves (a) and (b) in Fig. 3 represent the photoluminescence spectra of the nonirradiated crystal at a temperature $T = 80$ K and

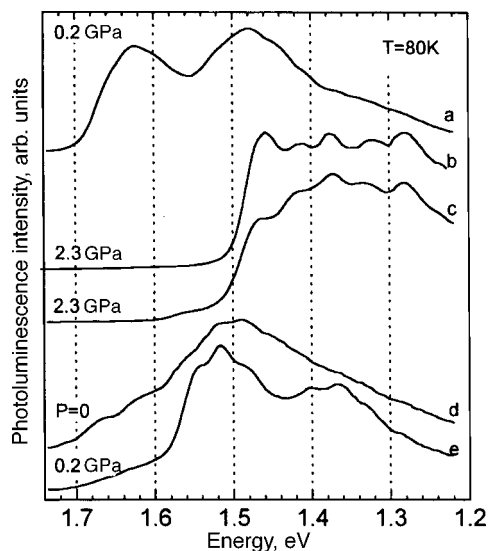


FIG. 3. Luminescence spectra of C_{60} crystals phototransformed at various pressures.

pressures of 0.2 GPa and 2.3 GPa, respectively. The crystal was then irradiated with light at the above-indicated power and duration at a pressure of 2.3 GPa and temperature $T = 200$ K. The photoluminescence spectrum of this crystal at $T = 80$ K is shown in Fig. 3(c). On the whole, its shape is quite close to that of the spectrum of the nonirradiated crystal (b) other than a certain broadening of the bands and diminution of the intensity of the short-wavelength C band. After the pressure is dropped back to the standard level the photoluminescence spectrum of this same crystal at $T = 80$ K acquires the form (d). It is evident from the figure that it is not similar to the initial spectrum (a), but is more like the characteristic spectrum (e) for the crystal preirradiated at standard pressure. The observable difference between spectra (d) and (e) is probably attributable to the presence of residual stresses in the crystal and cracking of the crystal after the pressure is dropped to the standard level, so that the spectral bands broaden, and the contribution of the initial spectrum increases somewhat. The results of the investigations show that spectrum (d) is stable against further irradiation of the crystal up to $T = 300$ K.

Consequently, the results indicate that when C_{60} crystals are irradiated by a laser beam in the temperature interval 180–240 K and at pressures up to 2.3 GPa, the photoluminescence spectra undergo a radical transformation as a result of restructuring of the radiative recombination X centers. At standard pressure this process attains its maximum efficiency at $T \cong 200$ K and falls off sharply near the point of transition to the orientationally disordered phase. The drop in efficiency of transformation of the centers at $T \geq 260$ K, when the molecules execute random rotation, is most likely indicative of the definite role played by the orientation of the C_{60} molecules during photoinduced transformation of the X centers.

In closing, the authors are grateful to R. K. Nikolaev for furnishing the C_{60} crystals, to the Russian Fund for Fundamental Research for partial financial support of the study (Project #99-02-17555), and to the NATO Research Committee for its support under the

auspices of the program “Collaboration Research” (HTECH.CRG #972317).

*¹Deceased.

¹W. Guss, J. Feldmann, E. O. Göbel *et al.*, Phys. Rev. Lett. **72**, 2644 (1994).

²V. V. Kveder, V. D. Negrii, É. A. Shteinman *et al.*, Zh. Éksp. Teor. Fiz. **113**, 734 (1998) [JETP **86**, 405 (1998)].

³K. P. Meletov and V. D. Negrii, JETP Lett. **68**, 248 (1998).

⁴P. A. Heiney, J. E. Fischer, A. R. McGhie *et al.*, Phys. Rev. Lett. **66**, 2911 (1991).

⁵C. Meingast and F. Gugenberger, Mod. Phys. Lett. B **B7**, 1703 (1993).

⁶A. M. Rao, P. Zhou, K.-A. Wang *et al.*, Science **259**, 955 (1993).

⁷I. O. Bashkin, A. P. Moravskii, E. G. Ponyatovskii *et al.*, JETP Lett. **59**, 279 (1994).

⁸Y. Iwasa, T. Arima, R. M. Fleming *et al.*, Science **264**, 1570 (1994).

⁹V. D. Negrii, V. V. Kveder, Yu. A. Ossipyan *et al.*, Phys. Status Solidi B **199**, 587 (1997).

¹⁰U. D. Venkateswaran, M. G. Schall, Y. Wang *et al.*, Solid State Commun. **96**, 951 (1995).

¹¹A. Jayaraman, Rev. Sci. Instrum. **57**, 1013 (1986).

¹²D. Barnett, S. Block, and G. J. Piermarini, Rev. Sci. Instrum. **44**, 1 (1973).

Translated by James S. Wood

Nonlinear interaction of magnetoacoustic waves in yttrium orthoferrite

B. A. Zon,^{*} and G. V. Pakhomov

Voronezh State University, 394693 Voronezh, Russia

(Submitted 11 November 1999)

Pis'ma Zh. Éksp. Teor. Fiz. **70**, No. 12, 789–792 (25 December 1999)

The phenomenon of energy transfer, both monotonic and oscillating, between the fundamental and higher harmonics of standing acoustic waves is observed during the laser generation of sound in YFeO_3 crystals. An analogous phenomenon for traveling light waves is well known in nonlinear optics. © 1999 American Institute of Physics.
[S0021-3640(99)00524-1]

PACS numbers: 72.55.+s, 43.35.Rw, 75.50.Dd, 43.25.Gf

Magnetoelastic interaction in weak ferromagnets produces an effective acoustic anharmonicity several orders of magnitude stronger than the intrinsic anharmonicity of the crystal. This phenomenon has been mentioned previously¹ and confirmed experimentally by the observation of elementary nonlinear effects: acoustic second-harmonic generation and demodulation in hematite^{2,3} and in thulium orthoferrite in the spin-flip region.⁴ Weak ferromagnets are therefore attractive for the observation of nonlinear acoustical effects. However, if high-power laser pulses are used to generate sound, it is possible to observe more complex nonlinear effects than those investigated in Refs. 2–4. We have used this technique in the present study.

The sound source was a laser beam having a wavelength of $1.064 \mu\text{m}$, a pulse duration of 15 ns, and a pulse energy up to 0.03 J. The diameter of the laser beam was 1.5 mm. The incidence of the pulsed laser beam on a magnetic crystal wafer produced very large strains ($>10^{-4}$) in it, which were then converted into a standing acoustic wave. Through magnetoelastic and piezomagnetic interactions the elastic vibrations induced corresponding oscillations of the magnetization of the crystal, which were recorded by an induction technique using a flat coil having a diameter 3.5 mm and consisting of 3–10 turns, which was placed directly on the surface of the sample. The laser beam passed through the central opening of the coil without touching its turns. This beam-coil configuration enabled us to record the time derivative of the magnetization increment ΔM in the direction of the z axis, which was perpendicular to the surface of the crystal. We have used a similar procedure in earlier work to observe the inverse Cotton–Mouton effect.⁵

The samples of yttrium orthoferrite single crystals comprised plane-parallel wafers cut perpendicular to the $[001]$ axis and perpendicular to the optical axis, with thicknesses $L=0.055–0.96$ mm and a base area $S \approx 0.5$ cm². The wafers were placed in an external magnetic field perpendicular to the plane of the crystal with an intensity $H \approx 500$ Oe,

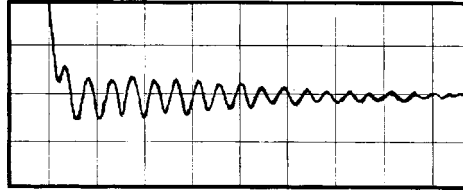


FIG. 1. Magnetoacoustic oscillations in a wafer of thickness 0.088 mm. Sweep 50 ns/div.

which was sufficient for attaining saturation of the magnetization. The laser beam was directed onto the sample surface at normal incidence. All the measurements were performed at room temperature.

The signal from the coil, amplified and displayed on the screen of an oscilloscope, consisted of two parts: an initial pulse matching the laser pulse in shape and duration, and an oscillating part associated with the standing acoustic wave. The initial pulse has previously been analyzed in detail⁶; here we confine our discussion to two remarks. First, both longitudinal and transverse acoustic modes can exist in the wafer, which acts as an acoustic resonator. For (001)-oriented samples the indicated procedure can be used to record the magnetization variation associated predominantly with longitudinal strains, but when the crystal is oriented perpendicular to the optical axis, the variation of the magnetization is attributable to both longitudinal and transverse strains.⁶ Second, if the sample has the same thickness as the flux linkage with the search coil, the total magnetic flux is zero for even-harmonic standing waves. This result is also associated with the identical boundary conditions on the front and back surfaces of the wafer (both surfaces can be regarded as free in our case). Even harmonics can contribute to the observed signal only when the thickness of the wafer is commensurate with the radius of the coil.

We now analyze the oscillating part of the signal. For test measurements we used thin wafers ($L=0.055$ mm and 0.135 mm, cut perpendicular to the [001] axis; $L=0.088$ mm and 0.117 mm, cut perpendicular to the optical axis), in which only the fundamental acoustic mode was efficiently generated. This condition is readily verified in light of the fact that for an YFeO_3 crystal and our choice of optical wavelength the absorption coefficient is $\approx 80 \text{ cm}^{-1}$. It is evident from Fig. 1 that the signal is a sine wave in this case. It also follows, therefore, that waves propagating parallel to the surface of the wafer (bulk and surface waves) do not contribute significantly to the observed signal. Numerical estimates of the acoustic wave velocities $v=2L/T$, where T is the period of the sine wave, give $v \approx (7 \pm 0.4) \times 10^5 \text{ cm/s}$ for the [001] direction and $v \approx (7.8 \pm 0.4) \times 10^5 \text{ cm/s}$ for the direction along the optical axis; these estimates are consistent with the velocities of longitudinal acoustic waves in an YFeO_3 crystal in the given directions.^{7,8}

For wafers with thicknesses $L=0.745$ mm, 0.80 mm, and 0.96 mm (cut perpendicular to the optical axis) several acoustic harmonics are generated with different relative strengths. As a result, the recorded signal has a complex profile, as exemplified by the oscillogram in Fig. 2. Clearly, after initial nonlinear distortions the signal evolves into an almost regular form of monochromatic oscillations, exhibiting a monotonic transfer of energy from the acoustic fundamental into the third harmonic (once again, even harmonics are not recorded by the procedure used here). This behavior is qualitatively described by the theory of nonlinear interaction of a finite set of harmonics as set forth in Refs. 9

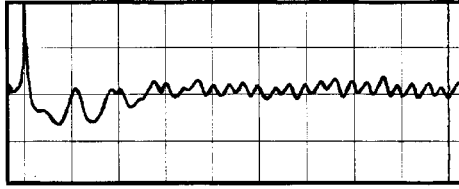


FIG. 2. Magnetoacoustic oscillations in a wafer of thickness 0.96 mm. Sweep 500 ns/div.

and 10. In our case this phenomenon can be identified both with nonlinear interaction between the transverse acoustic fundamental and second harmonics and with nonlinear interaction between the longitudinal and transverse acoustic fundamentals. In acoustics a similar phenomenon has been witnessed¹¹ as a monotonic decrease in the ratio of the intensities of the fundamental at the output and input of a MgO crystal.

An estimate of the wave velocity in the final part of the oscillogram gives $v \approx (4 \pm 0.2) \times 10^5$ cm/s, and a like estimate in the initial part gives $v \approx (4.4 \pm 0.2) \times 10^5$ cm/s, which is quite close to the transverse acoustic wave velocity.^{7,8}

The most interesting result from our point of view is the signal obtained for a wafer of thickness $L = 0.58$ mm cut perpendicular to the optical axis; see Fig. 3. The signal is seen as alternating oscillations of high and low frequencies. The only possible interpretation of such a signal is the periodic transfer of acoustic energy between the fundamental and higher harmonics. The transfer period is $T \approx 6 \mu\text{s}$.

A theoretical analysis shows¹² that the nonlinear interaction corresponding to energy transfer of both the monotonic kind shown in Fig. 2 and the oscillating process shown in Fig. 3 is attributable to the interaction of different acoustic modes. We know that two transverse acoustic modes having different polarizations and, in general, different velocities can propagate together with a longitudinal mode in the given direction in crystals. The small but definitely measurable difference in the sound velocities in the initial and final parts of the oscillogram in Fig. 2 cannot be attributed to frequency dispersion and indeed confirms the following interpretation: The nonlinear effects are caused by interaction between harmonics associated with different modes. The type of energy transfer — monotonic or oscillating — depends on the difference in the sound velocities of the differently polarized waves and the relative strengths of the fundamental and higher harmonics at the time when they are generated. These facts can account for the different types of energy transfer observed in Figs. 2 and 3, because wafers having thicknesses of 0.96 mm and 0.58 mm could also have had a small, uncontrollable difference in their orientations.

Unfortunately, the narrow range of variation of the laser intensity, limited by the

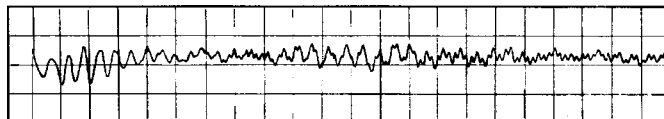


FIG. 3. Magnetoacoustic oscillations in a wafer of thickness 0.58 mm. Sweep 500 ns/div.

signal-to-noise ratio at one end and by the fracture threshold of the crystal at the other, made it impossible to measure the dependence of the type of energy transfer between acoustic modes on the acoustic power.

The authors are deeply grateful to Prof. N. Bloembergen and Prof. O. V. Rudenko for their interest in the study and for helpful comments, and also to L. D. Dorofeev, A. A. Krivchenkova, and V. Ya. Kupershmidt for many profitable discussions.

*)e-mail: zon@niif.vsu.ru

-
- ¹V. I. Ozhogin and V. L. Preobrazhenskii, *Zh. Éksp. Teor. Fiz.* **73**, 988 (1977) [*Sov. Phys. JETP* **46**, 523 (1977)].
 - ²V. I. Ozhogin, A. Yu. Lebedev, and A. Yu. Yakubovskii, *JETP Lett.* **27**, 313 (1978).
 - ³V. V. Berezhnov, N. N. Evtikhiev, V. L. Preobrazhenskii, and N. A. Ékonomov, *Akust. Zh.* **26**, 328 (1980) [*Sov. Phys. Acoust.* **26**, 180 (1980)].
 - ⁴A. Yu. Lebedev, V. I. Ozhogin, V. L. Safonov, and A. Yu. Yakubovskii, *Zh. Éksp. Teor. Fiz.* **85**, 1059 (1983) [*Sov. Phys. JETP* **58**, 616 (1983)].
 - ⁵B. A. Zon, V. Ya. Kupershmidt, G. V. Pakhomov, and T. T. Urazbaev, *JETP Lett.* **45**, 272 (1987).
 - ⁶A. M. Balbashov, B. A. Zon, V. Ya. Kupershmidt *et al.*, *Fiz. Tverd. Tela (Leningrad)* **29**, 1297 (1987) [*Sov. Phys. Solid State* **29**, 743 (1987)].
 - ⁷C. H. Tsang and R. L. White, *AIP Conf. Proc.* **24**, 749 (1975).
 - ⁸V. G. Bar'yakhtar, B. A. Ivanov, and M. V. Chetkin, *Usp. Fiz. Nauk* **146**, 417 (1985) [*Sov. Phys. Usp.* **28**, 563 (1985)].
 - ⁹N. Bloembergen, *Nonlinear Optics*, W. A. Benjamin, New York-Menlo Park, Calif. (1965), Chap. 4.
 - ¹⁰O. V. Rudenko and S. I. Soluyan, *Theoretical Foundations of Nonlinear Acoustics*, Consultants Bureau, New York (1977), Chap. 5.
 - ¹¹N. S. Shiren, *Appl. Phys. Lett.* **4**, 82 (1964).
 - ¹²D. L. Dorofeev, B. A. Zon, A. A. Krivchenkova, and G. V. Pakhomov, in *Nonlinear Solid-State Acoustics (Proceedings of the Eighth Meeting of the Russian Acoustical Society)* [in Russian], Nizhny Novgorod (1998), p. 197.

Translated by James S. Wood

Efficient nonlinear-optical frequency conversion in periodic media in the presence of diffraction of the pump and harmonic fields

V. A. Belyakov

*L. D. Landau Institute of Theoretical Physics, Russian Academy of Sciences,
117334 Moscow, Russia*

(Submitted 1 July 1999; resubmitted 18 November 1999)

Pis'ma Zh. Eksp. Teor. Fiz. **70**, No. 12, 793–799 (25 December 1999)

It has been predicted by Shelton and Shen [Phys. Rev. A **5**, 1867 (1972)] and observed by Kajikawa *et al.* [Jpn. J. Appl. Phys. Lett. **31**, L679 (1992)] and Yamada *et al.* [Appl. Phys. B **60**, 485 (1995)] that the efficiency of nonlinear-optical frequency conversion increases significantly in a nonlinear periodic medium and, accordingly, the intensity of the generated harmonic increases as the fourth power of the sample thickness, as opposed to the square law observed in homogeneous media. In this paper it is shown that the same enhancement of the efficiency of nonlinear-optical frequency conversion in a nonlinear periodic medium can be achieved using an ordinary pump wave in the form of a plane wave when both the pump wave and the harmonics are diffracted by the periodic structure of the nonlinear medium. The phenomenon is analyzed quantitatively in the example of second-harmonic generation. © 1999 American Institute of Physics.
[S0021-3640(99)00624-6]

PACS numbers: 42.65.Ky, 42.70.Nq

1. The nonlinear optics of periodic media has developed at a rapid pace in recent years.^{1–3} The new possibilities afforded by the nonlinear optics of periodic media beyond those of homogeneous media were first mentioned in Ref. 4. For the first time attention was focused primarily on the new possibilities of achieving phase matching in these media by virtue of the fact that the reciprocal lattice vector of a periodic structure can become a part of the phase matching conditions. Experiments on the implementation of such phase matching were reported in papers on second-harmonic generation in a solid-state periodic structure⁵ and on third-harmonic generation in cholesteric liquid crystals.⁶ It was later confirmed that the advantages of periodic media are also largely attributable to the theoretically predicted^{7,8} substantial increase in the efficiency of nonlinear-optical frequency conversion in them. Such efficiency improvement can be observed if the frequencies of the wave fields are close to the edges of the selective-reflection bands in periodic structures. It has been shown^{7–9} that definite relations between the parameters of the nonlinear medium must be established before this phenomenon can be achieved. In experimental work a major increase in the efficiency of second-harmonic generation has been observed¹⁰ under conditions such that the pump frequency is close to the selective-

reflection band edge in an artificially grown structure. Scalora *et al.*^{11,12} have arrived at the same conclusion of exceedingly large increase in the efficiency of second-harmonic generation in periodic media. Other authors^{7,8,12} have also discussed the conditions (relations between the optical parameters of the periodic medium, as well as the pump frequency) under which the efficiency of second-harmonic generation increases. The implementation of the necessary conditions poses a complex experimental problem; of utmost significance in this light, therefore, is a theoretical paper¹³ in which it has been shown that the efficiency of frequency conversion (with a harmonic intensity proportional to the fourth power of the sample thickness) can be increased, irrespective of the frequency dispersion of the dielectric permittivity (owing to the spatially variable component of the nonlinear susceptibility), by using a specially configured pump field (in the simplest case two counterpropagating waves).

A significant increase in the efficiency of second-harmonic generation has been observed^{14–16} in smectic liquid crystals when the harmonic frequency coincided with the band edge of selective light reflection in these chiral liquid crystals. The phase matching observed in Refs. 14–16 at the selective-reflection band edge was attributed to the onset of a standing wave of the pump field in the experiment, and it was postulated that in the presence of such a wave phase matching and an increase in the efficiency of nonlinear-optical frequency conversion could be achieved at the selective-reflection band edge independently of frequency dispersion of the permittivity.^{13,17,18} Specially designed experiments^{16,19} have confirmed the stated mechanism underlying the increased efficiency of nonlinear-optical frequency conversion.

2. The observed^{14–16,19} increase in the efficiency of nonlinear-optical frequency conversion should also be manifested in other kinds of periodic media and is of enormous practical interest. This consideration, in particular, lends a certain urgency to the search for new conditions amenable to the phenomenon in question. The immediate objective of the present study is to call attention to a new mechanism for improving the efficiency of nonlinear-optical frequency conversion with the achievement of phase matching at the selective-reflection band edge independently of frequency dispersion of the permittivity. We specifically address the feasibility of implementing the phenomenon in nonlinear periodic media in the presence of simultaneous diffraction of both the pump wave and the harmonic wave in the nonlinear medium. For definiteness we discuss the example of second-harmonic generation in a one-dimensionally periodic medium with harmonic modulation of the dielectric permittivity and nonlinear-optical characteristics. An analytical solution of the problem, ignoring pump attenuation, is obtained on the basis of dynamic diffraction theory.²⁰

3. We consider second-harmonic generation in a periodic medium with one-dimensional modulation of the dielectric permittivity ϵ and a quadratic nonlinear susceptibility χ of the form

$$\epsilon(z) = \epsilon_0 \{1 + \delta_1 \cos(\tau z + \varphi_1) + \delta_2 \cos(2\tau z + \varphi_2)\}, \quad (1)$$

$$\chi(z) = \chi_0 + \chi_1 \cos(\tau z + \varphi_n)\}. \quad (2)$$

We assume that a plane pump wave of frequency ω with wavevector $k(\omega)$ is incident at a grazing angle θ on a sample in the form of a plane-parallel plate of thickness L in a situation closely approximating the first-order diffraction scattering condition (see Fig. 1).

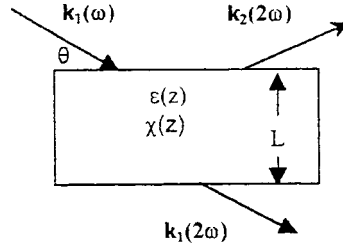


FIG. 1. Diagram of second-harmonic generation in the presence of diffraction of the wave fields.

The resulting second-harmonic wave exists under conditions closely approximating second-order diffraction scattering. The aim of the ensuing analysis is to disclose the conditions under which second-order diffraction occurs in the presence of phase matching for second-harmonic generation, knowing⁷⁻²¹ that this situation can lead to enhancement of the efficiency of second-harmonic generation.

To describe second-harmonic generation, it is necessary to solve the equation (which will be solved below in the two-wave approximation of dynamic diffraction theory²⁰)

$$\nabla \times \nabla \times \mathbf{E}(\mathbf{r}, 2\omega) - (2\omega/c)^2 \epsilon \mathbf{E}(\mathbf{r}, 2\omega) = (2\omega/c)^2 \chi : \mathbf{E}(\mathbf{r}, \omega) \mathbf{E}(\mathbf{r}, \omega), \quad (3)$$

where $\mathbf{E}(\mathbf{r}, 2\omega)$ and $\mathbf{E}(\mathbf{r}, \omega)$ are the second harmonic and pump fields, respectively.

Bearing in mind the above-stated assumption that the pump wave and the second harmonic are both diffracted, we can seek the harmonic and pump fields in the sample as superpositions of two plane waves, i.e., in the form (for the second harmonic as an example)

$$\mathbf{E}(\mathbf{r}, 2\omega) = (\mathbf{E}_1 \exp[i\mathbf{k}_1 \cdot \mathbf{r}] + \mathbf{E}_2 \exp[i\mathbf{k}_2 \cdot \mathbf{r}]) \exp[-i2\omega t], \quad (4)$$

where $\mathbf{k}_2 - \mathbf{k}_1 = 2\boldsymbol{\tau}$, and $\boldsymbol{\tau}$ is the reciprocal lattice vector of the periodic structure. Substituting Eq. (4) and the corresponding expression for the pump field into Eq. (3), we obtain the following system of equations for the amplitudes of the harmonic field:

$$\begin{aligned} (1 - (k_1/\kappa)^2)E_1 + \delta_2 E_2 &= -(4\pi/\epsilon) \mathbf{P}_0 \delta(\mathbf{k}_1 - 2\mathbf{k}(\omega)), \\ \delta_2 E_1 + (1 - (k_2/\kappa)^2)E_2 &= -(4\pi/\epsilon) \mathbf{P}_\tau \delta(\mathbf{k}_2 - 2\mathbf{k}(\omega)), \end{aligned} \quad (5)$$

where \mathbf{P}_0 and \mathbf{P}_τ are the Fourier harmonics in the expansion of the nonlinear polarization. To simplify the derivation of Eqs. (5), we have assumed that the pump wave is linearly polarized perpendicular to the scattering plane.

Inasmuch as the pump field in the presence of diffraction is written in a form analogous to Eq. (4), to achieve phase matching independent of frequency dispersion of the dielectric characteristics of the sample,¹³ it is sufficient to assume, by analogy with Ref. 13, that only the spatially modulated component of the nonlinear susceptibility (2) contributes to the nonlinear polarizations in Eqs. (5), and plane waves represented by expressions of the type (4) have been substituted into the products of the wave fields on the right-hand side of Eq. (3). Here the components of the harmonic wavevectors in the same direction as the periodicity in Eq. (4) are very close to $\pm \tau$, implying the occurrence of second-order diffraction scattering.

To investigate the phase matching conditions, we rely on the convenience of standard parametrization of the solution in solving Eqs. (5) for the fundamental and harmonic waves. For example, we use the following relations for the pump wave:

$$k_{1n}(\omega) = -(\tau/2)(1 + \alpha_1), \quad \nu_1 = 1 - [(\tau/2)^2 + (k_{\perp}(\omega))^2]/(\kappa(\omega))^2, \quad (6)$$

where $k_{1n}(\omega)$ and $k_{\perp}(\omega)$ are the components of the pump wavevector parallel and perpendicular to the periodicity direction, respectively.

By solving a system of equations analogous to the homogeneous system corresponding to (5), we obtain the following expression for α_1 :

$$\alpha_{1\pm} = \pm(\nu_1^2 - \delta_1^2)^{1/2}/(2(\nu_1 + \sin^2 \theta)), \quad (7)$$

Introducing an analogous parametrization for the harmonic (α_2 and ν_2) and the notation $\eta = 1 - \epsilon_{\omega}/\epsilon_{2\omega}$, from the condition of continuity of the tangential components of the wavevectors we find a relation between the parameters of the pump and harmonic waves:

$$\nu_2 = \nu_1(1 - \eta) - \eta. \quad (8)$$

The solution of the system (5) for the harmonic represents the superposition of the particular solution of this system with the normal modes of the corresponding homogeneous system with wavevectors governed by the parameter ν_2 . But the wavevector in the particular solution is governed by the δ functions on the right-hand sides of this system, whence it follows that its component parallel to the periodicity direction is given by the expression

$$k_{in} = -\tau - (\tau/2)(\alpha_{1\pm} + \alpha_{1\pm}), \quad (9)$$

where all combinations of signs for $\alpha_{1\pm}$ are admissible on the right-hand side of the equation.

4. The phase matching condition stipulates that the wavevector (9) of the particular solution coincide with the wavevector of at least one normal mode, i.e.,

$$(\nu_2)^2 - (\tau/k(2\omega))^4(\alpha_{1+} + \alpha_{1-})^2 - (\delta_2)^2 = 0. \quad (10)$$

By virtue of Eqs. (6)–(8), Eq. (10) gives the value of the parameter ν_1 corresponding to phase matching, i.e., the deviation of the angle of incidence of the pump wave from the exact Bragg angle or, at a fixed angle of incidence, the deviation of the pump frequency from its exact Bragg value. To maximize the efficiency of second-harmonic generation, it is necessary that phase matching be attained precisely at the selective-reflection band edge for the harmonic. The corresponding condition is given by the additional requirement $\nu_2 = \pm \delta_2$. This situation occurs, in particular, if the expression in the parentheses in Eqs. (9) and (10) is $\alpha_{1+} + \alpha_{1-}$, which is identically zero. The corresponding value of the pump parameter ν_1 for phase matching is determined from Eq. (8) by substituting $\nu_2 = \pm \delta_2$ therein, i.e., by setting $\nu_1 = (\pm \delta_2 + \eta)/(1 - \eta)$. If the quantity $\alpha_{1\pm} + \alpha_{1\pm}$ in Eq. (10) is not identically zero, phase matching with respect to the parameter ν_2 is achieved, in general, irrespective of selective reflection, and the corresponding value of ν_1 , denoted by ν_{1p} , is given by the relation

$$\nu_{1p} = -(\delta_1^2(1 - \eta)^2 - \delta_2^2 + \eta^2)/(2(1 - \eta)\eta). \quad (11)$$

It is important to note here that the magnitude of the nonlinear polarization on the right-hand side of Eq. (3) varies considerably in the given situation for small deviations of the pump wave from the exact Bragg condition.

5. The nonlinear polarization on the right-hand side of Eq. (3) is proportional to a quadratic combination of the amplitudes of the normal modes superimposed to form the pump wave in the sample. These amplitudes exhibit different dependences on the thickness of the sample and are given by the equations

$$\begin{aligned} C_+ &= [E_0 \xi_{1-} \exp(i\alpha_{1-}l/2)] / (\xi_{1-} \exp(-i\alpha_{1-}l/2) - \xi_{1+} \exp(i\alpha_{1+}l/2)), \\ C_- &= [E_0 \xi_{1+} \exp(i\alpha_{1+}l/2)] / (\xi_{1-} \exp(-i\alpha_{1-}l/2) - \xi_{1+} \exp(i\alpha_{1+}l/2)), \end{aligned} \quad (12)$$

where E_0 is the amplitude of the pump wave outside the sample, $l = \tau L$ is the dimensionless thickness of the sample, $\xi = E_2/E_1$ is the ratio of the amplitudes of the two plane waves comprised in the normal mode, $\alpha_{1\pm}$ is given by Eq. (7), the plus sign in subscripts refers to a normal mode that decays into the depth of the sample, and the minus sign refers to a normal mode that grows in the direction from the entrant surface of the sample. As the sample thickness tends to infinity, we have $C_+ = E_0$ and $C_- = 0$. Since the phase matching condition (10) involves the quantities $\alpha_{1\pm} + \alpha_{1\pm}$ in various combinations, for different phase matching conditions (10) the nonlinear polarizations in Eq. (3) are proportional to different combinations of the coefficients C_{\pm} . In light of the previously mentioned appreciable difference in the dependence of the coefficients C_{\pm} on the thickness, the same is true of the intensity of second-harmonic generation for the separate components of the nonlinear polarization.

6. Finally, we obtain the following equations for the amplitudes of the harmonics emanating from the exit and entrant surfaces of the sample:

$$\begin{aligned} E_1(z=L) &= \{e_0 \exp(i(\alpha_{1+} + \alpha_{1-})l/2) + [e_0(\xi_+ - \xi_-) \\ &\quad + 2ie_1 \sin(\alpha_2 l) / (\xi_- \exp(-i\alpha_2 l) - \xi_+ \exp(i\alpha_2 l))]\} / D, \\ E_2(z=0) &= \{e_1 + [e_1(\xi_+ - \xi_-) + 2ie_0 \sin(\alpha_2 l) / (\xi_- \exp(-i\alpha_2 l) \\ &\quad - \xi_+ \exp(i\alpha_2 l))]\} / D, \end{aligned} \quad (13)$$

where $\alpha_2 = (\nu_2^2 - \delta_2^2)^{1/2} / (2(\nu_2 + \sin^2 \theta))$, and ν_2 is related to ν_1 by Eq. (8);

$$\begin{aligned} \xi_{\pm} &= -\delta_2 / [\nu_2 \pm \alpha_2], \quad D = \nu_2^2 - (\tau/k(2\omega))^4 (\alpha_{1+} + \alpha_{1-})^2 - \delta_2^2, \\ \nu_2 &= 1 - [(\tau)^2 + (2k_{\perp}(\omega))^2] / (\kappa(2\omega))^2, \\ e_0 &= -[(\nu_2 + (\tau/k(2\omega))^2 (\alpha_{1+} + \alpha_{1-})) P_0 - P_{\tau} \delta_2], \\ e_1 &= -[(\nu_2 - (\tau/k(2\omega))^2 (\alpha_{1+} + \alpha_{1-})) P_{\tau} - P_0 \delta_2], \end{aligned} \quad (14)$$

and the quantities P_0 and P_{τ} , according to Eqs. (3) and (5), are expressed in terms of χ_1 and products of C_{\pm} .

7. We now give the results of numerical calculations for specific values of the parameters of the problem. The following values of the parameters are used in the calculations: $\delta_1 = 0.07$, $\delta_2 = 0.057$, $\theta = \pi/6$, $\eta = 0.001$, and it is assumed that the permittivity outside the sample coincides with the average permittivity of the sample.

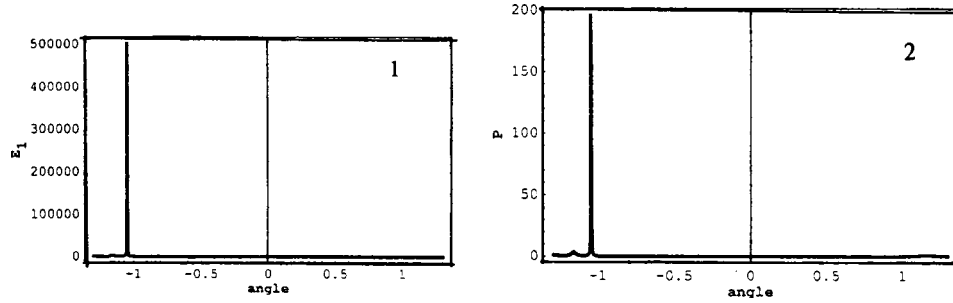


FIG. 2. Dependence of the second-harmonic generation amplitude E_1 (1) and the corresponding nonlinear polarization P_{+-} (2) on the parameter ν_1/δ_1 (at a fixed pump frequency this graph corresponds to the dependence on the proximity of the pump wave to the Bragg condition with respect to its angle of incidence) for a sample of thickness $l=100$ (E_2 is equal to E_1 in this case).

Figures 2 (graph 2), 4 (graph 3), and 5 (graph 3) show the behavior of the nonlinear polarizations for deviations of the pump wave from the Bragg condition. The polarizations P_{++} , P_{+-} , P_{--} rise sharply at the selective-reflection band edge of the pump wave. The calculations of the second-harmonic generation amplitude for the polarization P_{+-} Figs. 2 (graph 1) and 3 (graph 1) show that its maximum occurs near the selective-reflection band edge for the doubled frequency independently of frequency dispersion, i.e., under conditions conducive to enhancement of the efficiency of second-harmonic generation.^{7-9,13,17,18} The graphs of the amplitudes as functions of ν_1 can also have maxima when ν_1 corresponds to the selective-reflection band edge for the pump wave. The dependence of the second-harmonic generation amplitude on the sample thickness is shown in Fig. 3 (graph 1), which, as expected, gives a maximum of the second-harmonic generation amplitude for a finite sample thickness.

In general, the other phase matching conditions corresponding to the nonlinear polarizations P_{--} and P_{++} lead to phase matching far from the selective-reflection band edge (see Fig. 4). For phase matching to be achieved near the selective-reflection band edge the parameters of the nonlinear periodic medium must satisfy certain relations, deduced from Eqs. (8) and (11), between the parameters of the nonlinear periodic medium. The coincidence of the phase matching conditions with the selective-reflection

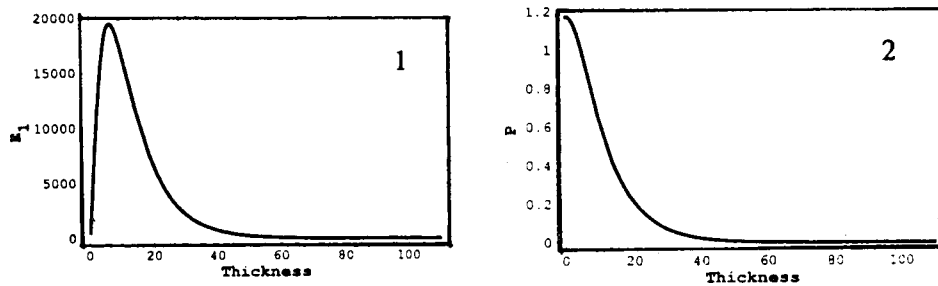


FIG. 3. Dependence of the second-harmonic generation amplitude (in arbitrary units) E_1 (1) ($E_2=E_1$) and the corresponding nonlinear polarization P_{+-} (2) on the sample thickness for the parameter $\nu_1/\delta_1=-0.81$.

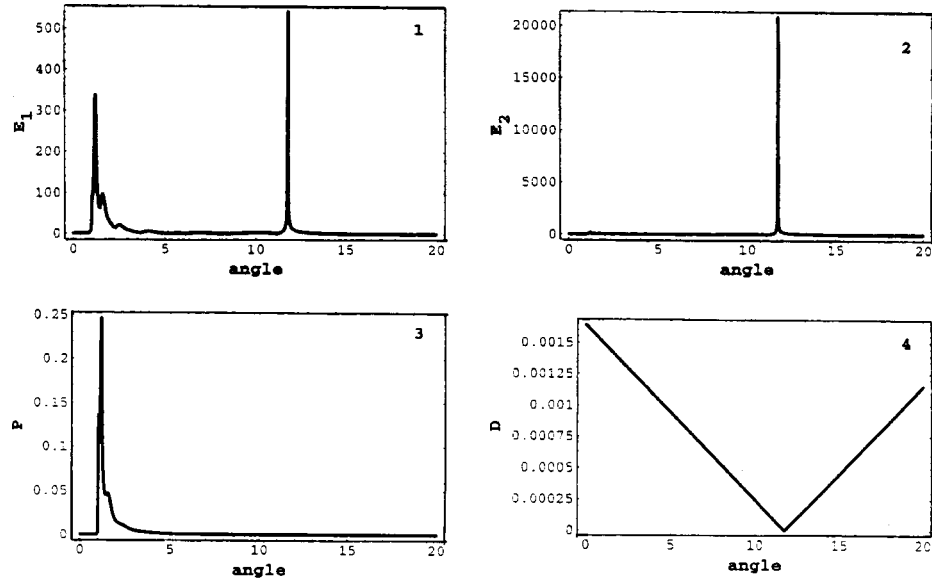


FIG. 4. Dependence of the second-harmonic generation amplitudes (in arbitrary units) E_1 (1) and E_2 (2) and the corresponding nonlinear polarizations P_{--} (3, 4) of the modulus of expression (10) on the parameter ν_1/δ_1 for $l=100$.

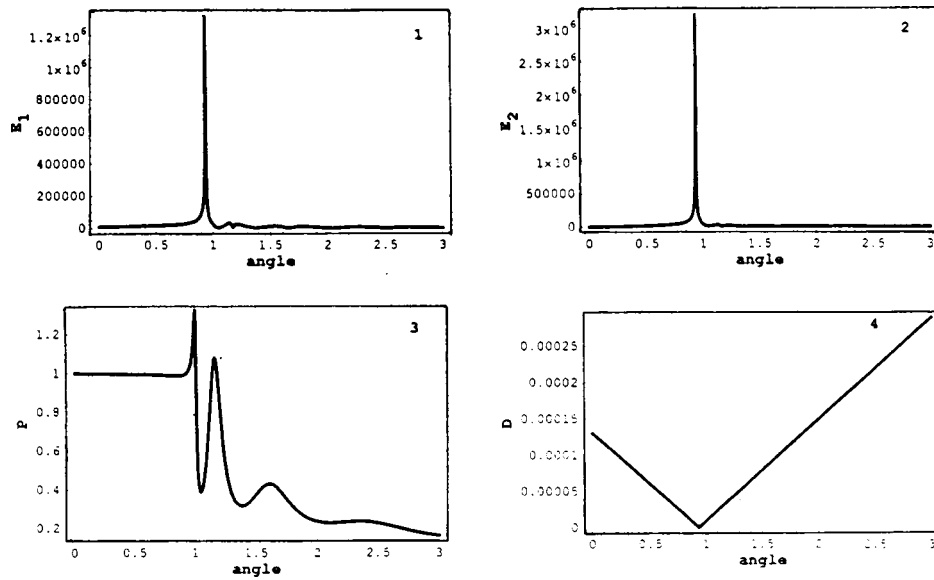


FIG. 5. Dependence of the second-harmonic generation amplitudes (in arbitrary units) E_1 (1) and E_2 (2) and the corresponding nonlinear polarizations P_{++} (3, 4) of the modulus of expression (10) on the parameter ν_1/δ_1 for $l=100$ and the value of the parameter $\delta_2=0.0691$ for phase matching at the selective-reflection band edge.

band edge in this case and the high efficiency of second-harmonic generation are illustrated by Fig. 5, which shows the results of calculations for almost identical values of the parameters δ_1 and δ_2 .

8. The foregoing results demonstrate the possibilities for achieving highly efficient nonlinear-optical frequency multiplication in nonlinear periodic media in the presence of diffraction of the fundamental and harmonic fields. Despite our investigation of the problem in the example of second-harmonic generation for a simple model of a nonlinear periodic medium, the qualitative results pertaining to the increased efficiency of nonlinear-optical frequency conversion have more general implications and are applicable both to other types of periodic media and to other nonlinear frequency multiplication processes (see, e.g., Ref. 8).

- ¹R. L. Byer, *Nonlinear Opt.* **7**, 235 (1999).
- ²A. S. Chirkin and V. V. Volkov, *J. Russ. Laser Res.* **19**, 409 (1998).
- ³A. V. Andreev, O. A. Andreeva, A. V. Balakin *et al.*, *Kvantovaya Elektron.* **28**, 75 (1999).
- ⁴N. Bloembergen and A. J. Sievers, *Appl. Phys. Lett.* **17**, 483 (1970).
- ⁵J. P. van Der Ziel and M. Ilegems, *Appl. Phys. Lett.* **28**, 437 (1976).
- ⁶J. W. Shelton and Y. R. Shen, *Phys. Rev. A* **5**, 1867 (1972).
- ⁷V. A. Belyakov and N. V. Shipov, *Phys. Lett. A* **86**, 94 (1981).
- ⁸V. A. Belyakov and N. V. Shipov, *Zh. Eksp. Teor. Fiz.* **82**, 1159 (1982) [*Sov. Phys. JETP* **55**, 674 (1982)].
- ⁹S. V. Shiyankovskii, *Ukr. Fiz. Zh. (Russ. Ed.)* **27**, 361 (1982).
- ¹⁰S. Nakagawa, N. Yamada, N. Mikoshiba *et al.*, *Appl. Phys. Lett.* **66**, 2159 (1995).
- ¹¹M. Scalora, M. J. Bloemer, A. S. Manka *et al.*, *Phys. Rev. A* **56**, 3166 (1997).
- ¹²J. W. Haus, R. Viswanathan, M. Scalora *et al.*, *Phys. Rev. A* **57**, 2120 (1998).
- ¹³V. A. Belyakov and N. V. Shipov, *Pis'ma Zh. Tekh. Fiz.* **9**, 22 (1983) [*Sov. Tech. Phys. Lett.* **9**, 9 (1983)].
- ¹⁴K. Kajikawa, T. Isozaki, H. Takezoe *et al.*, *Jpn. J. Appl. Phys., Part 2* **31**, L679 (1992).
- ¹⁵T. Furukawa, T. Yamada, K. Ishikawa *et al.*, *Appl. Phys. B* **60**, 485 (1995).
- ¹⁶J. Yoo, S. Choi, H. Hoshi *et al.*, *Jpn. J. Appl. Phys., Part 2* **36**, L1168 (1997).
- ¹⁷M. Copic and I. Drevensek-Olenik, *Liq. Cryst.* **21**, 233 (1996).
- ¹⁸I. Drevensek-Olenik and M. Copic, *Phys. Rev. E* **56**, 581 (1997).
- ¹⁹D. Chung *et al.*, 1999 (in press).
- ²⁰V. A. Belyakov, *Diffraction Optics of Complex-Structured Periodic Media*, Springer-Verlag, Berlin-New York (1992).
- ²¹S. V. Shiyankovskii, *SPIE Proc.* **2795**, 2 (1996).

Translated by James S. Wood

Matched second-harmonic generation of ultrashort laser pulses in photonic crystals

A. V. Tarasishin, A. M. Zheltikov, and S. A. Magnitskiĭ

International Laser Center, M. V. Lomonosov Moscow State University, 119899 Moscow, Russia

(Submitted 15 November 1999)

Pis'ma Zh. Éksp. Teor. Fiz. **70**, No. 12, 800–805 (25 December 1999)

It is shown that one-dimensional photonic bandgap structures are capable of simultaneously satisfying the phase and group-velocity matching conditions for second-harmonic generation involving extremely short light pulses. When these conditions are satisfied, an optical frequency doubler utilizing photonic bandgap structures provides a means for increasing the rate of growth of the second-harmonic signal as a function of the nonlinear-optical interaction length relative to structures designed for quasi-matched interactions and affords possibilities for enhancing the frequency doubling efficiencies independently of the matching length in the bulk nonlinear material. © 1999 American Institute of Physics. [S0021-3640(99)00724-0]

PACS numbers: 42.70.Qs, 42.65.Ky, 42.65.Re

To increase the efficiency of frequency conversion is a long-standing goal of nonlinear optics.^{1,2} Today the widespread proliferation of compact, low-cost femtosecond solid-state laser systems and the enormous difficulties encountered in doubling the frequency of ultrashort laser pulses underscore the impact of new possibilities for enhancing the efficiency of second-harmonic generation in application to extremely short light pulses. One of the foremost basic problems of second-harmonic generation for ultrashort laser pulses is the need to achieve phase and group-velocity matching. Periodically inhomogeneous crystals, in which quasi-phase-matched interaction conditions are achieved by modulating the quadratic susceptibility of the medium with a spatial period of the order of the coherent nonlinear-optical interaction length,^{3,4} are widely used nowadays to enhance the efficiency of second-harmonic generation (the concept of quasi-phase matching was proposed years ago in a 1962 groundbreaking paper on nonlinear optics⁵).

The feasibility of increasing the efficiency of second-harmonic generation by establishing phase matching in one-dimensional structures with photonic bandgaps, i.e., photonic crystals, is a topic of heated discussion at the present time.^{6,7} In contrast with crystals used for quasi-matched interaction, photonic bandgap structures are characterized by spatially periodic modulation of the refractive index rather than the nonlinear-optical susceptibility. The characteristic space scale of the variation of the refractive index in photonic bandgap structures is of the order of the optical wavelength, i.e., it is significantly smaller than the modulation period of the nonlinear-optical susceptibility in struc-

tures used for quasi-matched interaction. The notion of utilizing the dispersion of periodic structures to compensate the material dispersion of the medium as a means of establishing phase matching conditions for second-harmonic generation and nonlinear-optical frequency shifting was advanced some time ago.⁸ At the present stage of nonlinear optics, however, the simultaneous implementation of group-velocity and phase matching conditions poses a timely objective in connection with the frequency conversion problem for ultrashort laser pulses. This paper addresses the solution of the stated problem.

To illustrate the concept of second-harmonic generation in a field of ultrashort pulses in photonic crystals with phase and group-velocity matched photonic crystals, we consider the dispersive properties of a model infinite photonic bandgap structure consisting of periodically alternating layers with dimensions a and b and refractive indices n_a and n_b , respectively. It will be shown below by comparing the results of analytical calculations with numerical data that the model of an infinite photonic bandgap structure affords the capability of adequately reproducing the basic properties of nonlinear-optical interactions involving comparatively short pulses when the number of periods of the field in the pulse is much smaller than the number of periods of the photonic bandgap structure. We assume that the layers with index n_b are endowed with quadratic nonlinearity, which leads to second-harmonic generation. We first consider the case of second-harmonic generation in a one-dimensional photonic bandgap structure without dispersion on the part of the materials constituting the structure; we then generalize these results to photonic bandgap structures with material dispersion taken into account.

The phase matching condition for the wavevectors $k(\omega_0)$ and $k(2\omega_0)$ of the pump and second-harmonic waves involved in the process of second-harmonic generation are written in the form

$$k(2\omega_0) = 2k(\omega_0). \quad (1)$$

The wavevectors at the fundamental and the second-harmonic frequencies can be determined from the dispersion relation for the investigated infinite one-dimensional photonic bandgap structure:

$$\cos(k(\omega_0)d) = \cos\left(\frac{\omega_0}{c}n_a a\right) \cos\left(\frac{\omega_0}{c}n_b b\right) - \frac{n_a^2 + n_b^2}{2n_a n_b} \sin\left(\frac{\omega_0}{c}n_a a\right) \sin\left(\frac{\omega_0}{c}n_b b\right), \quad (2)$$

$$\cos(k(2\omega_0)d) = \cos\left(\frac{2\omega_0}{c}n_a a\right) \cos\left(\frac{2\omega_0}{c}n_b b\right) - \frac{n_a^2 + n_b^2}{2n_a n_b} \sin\left(\frac{2\omega_0}{c}n_a a\right) \sin\left(\frac{2\omega_0}{c}n_b b\right). \quad (3)$$

Taking Eqs. (2) and (3) into account, we can write the phase matching condition (1) in the form

$$\cos^2(Ak_0) + \cos^2(Bk_0) - \cos^2(Ak_0)\cos^2(Bk_0) = 1, \quad (4)$$

where $k_0 = \omega_0/c$, and we have introduced the notation $A = n_a a$, $B = n_b b$, $N = (n_a^2 + n_b^2)/2n_a n_b$.

Equation (4) is satisfied if and only if one of the cosines squared is equal to unity. Assuming for definiteness that $\cos^2(Ak_0) = 1$, we obtain

$$a = \lambda/2n_a, \quad (5)$$

where l is an integer.

Consequently, when one of the subsystems of the infinite one-dimensional photonic bandgap structure is a set of half-wave plates, i.e., when the parameter a is chosen according to Eq. (5), phase matching is always achieved for second-harmonic generation. We now show that the group-velocity matching condition is automatically satisfied as well in this case:

$$\left. \frac{\partial k(\omega)}{\partial \omega} \right|_{\omega=\omega_0} = \left. \frac{\partial k(\omega)}{\partial \omega} \right|_{\omega=2\omega_0}. \quad (6)$$

When condition (5) holds, the reciprocal group velocities at the fundamental and second-harmonic frequencies can be written as follows on the basis of Eqs. (2) and (3):

$$\left. \frac{\partial k(\omega)}{\partial \omega} \right|_{\omega=\omega_0, 2\omega_0} = \frac{\pm(B+AN)}{cd}. \quad (7)$$

Allowing for the fact that waves transmitted through the photonic bandgap structure correspond to positive values of the group velocity, we find that the group-velocity matching conditions are also satisfied for a nondispersive photonic bandgap structure with parameters satisfying Eq. (5).

We now extend the above results to a photonic bandgap structure in which not only the dispersion of the structure, but also the dispersion of the medium must be taken into account, and we determine the phase and group-velocity matching conditions for this case. For simplicity we consider a photonic bandgap structure consisting of layers of thickness a with a refractive index n_a , no nonlinearity, and negligible dispersion, alternating with quadratically nonlinear layers of thickness b with a frequency-independent refractive index n_b . In this case the wavevectors at the pump and second-harmonic frequencies can be written in the form

$$\cos(k(\omega_0)d) = \cos\left(\frac{\omega_0}{c}n_a a\right) \cos\left(\frac{\omega_0}{c}n_{1b} b\right) - \frac{n_a^2 + n_{1b}^2}{2n_a n_{1b}} \sin\left(\frac{\omega_0}{c}n_a a\right) \sin\left(\frac{\omega_0}{c}n_{1b} b\right), \quad (8)$$

$$\cos(k(2\omega_0)d) = \cos\left(\frac{2\omega_0}{c}n_a a\right) \cos\left(\frac{2\omega_0}{c}n_{2b} b\right) - \frac{n_a^2 + n_{2b}^2}{2n_a n_{2b}} \sin\left(\frac{2\omega_0}{c}n_a a\right) \sin\left(\frac{2\omega_0}{c}n_{2b} b\right). \quad (9)$$

Here n_{1b} and n_{2b} are the refractive indices of the nonlinear medium at the pump and second-harmonic frequencies, respectively. The phase matching condition is the same as before; see Eq. (1).

The reciprocal group velocities of the pump and second-harmonic pulses are given by the equations

$$\begin{aligned} \left. \frac{\partial k(\omega)}{\partial \omega} \right|_{\omega=\omega_0} &= \frac{1}{cd \sin(k(\omega_0)d)} ((B_1 + AN_1) \cos(Ak_0) \\ &\quad \times \sin(B_1 k_0) + (A + B_1 N_1) \sin(Ak_0) \cos(B_1 k_0)), \end{aligned} \quad (10)$$

$$\left. \frac{\partial k(\omega)}{\partial \omega} \right|_{\omega=2\omega_0} = \frac{1}{cd \sin(k(2\omega_0)d)} ((B_2 + AN_2) \cos(Ak_0) \times \sin(B_2k_0) + (A + B_2N_2) \sin(Ak_0) \cos(B_2k_0)), \quad (11)$$

where $A = n_a a$, $B_{1,2} = n_{1,2b} b$, and $N_{1,2} = (n_a^2 + n_{1,2b}^2) / 2n_a n_{1,2b}$. The group-velocity matching condition is written in the form (6).

Consequently, the condition for efficient second-harmonic generation in a one-dimensional photonic bandgap structure with material dispersion and negligible group-velocity dispersion stipulates the simultaneous satisfaction of Eq. (1) for the quantities (8) and (9) and of Eq. (6) for the quantities (10) and (11). For a given pump wavelength and given values of the refractive indices n_a , n_{1b} , and n_{2b} the indicated system of two equations (1) and (6) can be solved for the parameters a and b . It is therefore possible for the phase and group-velocity matching conditions to be satisfied simultaneously. It is obvious, however, that the transcendental system of equations does not have a solution for all values of the refractive indices n_a , n_{1b} , and n_{2b} . In particular, it is readily verified by direct substitution of the values of a given by condition (5) into (10) and (11) that phase matching is impossible in a photonic bandgap structure in which one of the subsystems is a set of half-wave plates and in which the nonlinear medium exhibits dispersion of the refractive index.

From the physical standpoint phase and group-velocity matching for second-harmonic generation in a photonic bandgap structure containing a nonlinear material characterized by dispersion of the refractive index is achieved as a result of compensation of the material dispersion by the dispersion of the periodic structure. Consequently, increasing the dispersion of the nonlinear medium to compensate the attendant increase of the phase and group-velocity mismatches requires ever-increasing contrast of the refractive index of the media constituting the photonic bandgap structure. The dependence of the minimum contrast n_{1b}/n_a of the refractive indices such for the existence of a simultaneous solution of the system of equations (1), (6) on the quantity $(n_{2b} - n_{1b})/n_{1b}$, which represents the difference between the refractive indices of the nonlinear medium at the second-harmonic and fundamental frequencies, normalized to the latter index, can be determined by solving the system of equations numerically by the gradient method. This dependence for a photonic bandgap structure with $n_{1b} = 1.5$ is plotted in Fig. 1. It is evident from the results of the calculations shown in this figure that the dispersion of photonic bandgap structures with index contrasts obtainable by existing technologies can be exploited to compensate the phase and group-velocity mismatches for second-harmonic generation over a fairly broad range of dispersion of the nonlinear medium.

The calculation of the amplitude of the second-harmonic field produced by the second-harmonic generation process in a photonic bandgap structure poses a complex physical problem. We have therefore calculated numerically the amplitude of the second harmonic resulting from the second-harmonic generation process by solving Maxwell's equations numerically using the finite-difference time-domain (FDTD) algorithm.⁹ This approach is an effective method for the analysis of nonlinear-optical interactions involving ultrashort light pulses in photonic crystals.¹⁰

The FDTD method for a cubically nonlinear, dispersive medium is described in Ref.

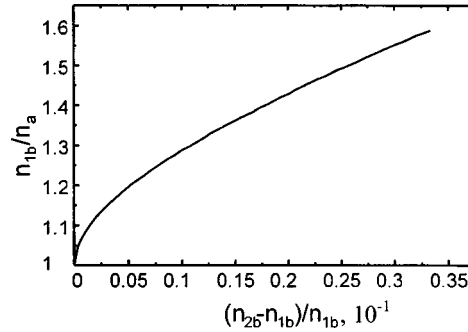


FIG. 1. Dependence of the minimum contrast n_{1b}/n_a of the refractive indices for simultaneous satisfaction of the phase and group-velocity matching conditions (1) and (6) on the quantity $(n_{2b}-n_{1b})/n_{1b}$.

11. We have implemented the FDTD algorithm for a quadratically nonlinear medium with local response of the nonlinearity and dispersion of the dielectric permittivity described by a Lorentzian line profile: $\epsilon(\omega) = \epsilon_\infty + (\epsilon_s - \epsilon_\infty)/(1 - \omega^2/\omega_L^2)$, where ω_L is the resonance frequency, ϵ_∞ is the permittivity of the medium in the high-frequency limit, and ϵ_s is the permittivity of the medium in the low-frequency limit.

Without frequency dispersion the maximum efficiency of second-harmonic generation is attained in a structure with the parameters

$$a = \lambda/2n_a, \quad b = \lambda/4n_b. \quad (12)$$

This result is fully consistent with the above analytical investigation for an infinite one-dimensional structure. The first of the equations (12) establishes phase and group-velocity matching, and it is readily shown by means of Eqs. (2) and (3) that the second condition stipulates zero dispersion of the group velocity at the fundamental and second-harmonic frequencies. A numerical simulation for Gaussian pulses of extremely short duration propagating in a photonic bandgap structure with $n_a = 2$ and $n_b = 1$ has shown that when conditions (12) are satisfied, the dependence of the second-harmonic generation efficiency (defined as the ratio of the energy of the second-harmonic pulses at the output of the photonic bandgap structure to the pump energy at the input) on the length of the structure is close to quadratic at wavelengths of the order of $1 - 10^3$ periods of the structure for pulses having a duration τ equal to at least ten periods of the pump field (solid curve in Fig. 2). For shorter durations, such that the width of the pulse spectrum becomes of the same order or greater than that of the range of allowed photon energies, the second-harmonic generation efficiency increases far more slowly than the square of the length of the photonic bandgap structure (dashed and dotted curves in Fig. 2). This effect is attributable to the inability of the phase and group-velocity matching conditions to be satisfied over such a broad spectral range. Another significant factor for short pulses is dispersion spreading of the pulse, because the dispersion of higher orders attains large values near the band edge.

As mentioned above, the matching technique for nonlinear-optical interactions in photonic bandgap structures is fundamentally different in nature from the matching in structures for quasi-phase-matched interactions. The quasi-matched interaction regime is established by changing the sign of the quadratic susceptibility of the nonlinear material

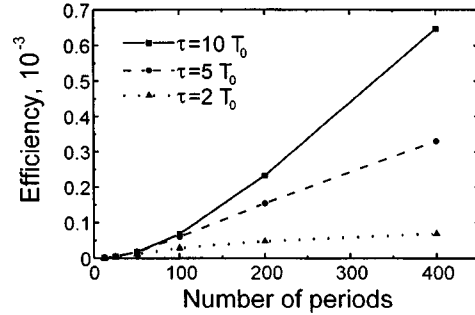


FIG. 2. Dependence of the efficiency of second-harmonic generation on the number of periods of a photonic bandgap structure for pulses of various durations: $\tau = 10T_0$ (solid curve); $5T_0$ (dashed curve); $2T_0$ (dotted curve); (T_0 is the period of the pump field).

within a characteristic space scale of the order of the coherence length. A typical graph of the second-harmonic generation efficiency as a function of the length of the nonlinear medium for the given frequency conversion regime is represented by the dot-dash curve in Fig. 3. Matched second-harmonic generation in photonic bandgap structures is established by modulating the refractive index over a characteristic space scale smaller than the optical wavelength, a technique that permits both phase matching and group-velocity matching and affords possibilities for attaining high second-harmonic generation efficiencies independently of the matching length in the bulk nonlinear material. This consideration is of utmost importance in regard to practical applications.

A major difference in the phase-locked second-harmonic generation regime proposed in this paper for photonic bandgap structures from the second-harmonic generation regime discussed in Refs. 6 and 7 for photonic crystals is that the width of the spectral range of efficiency second-harmonic generation in our case is not restricted by the resonance width in the transmission spectrum of a one-dimensional photonic bandgap structure with a finite number of periods. Because one-dimensional photonic bandgap struc-

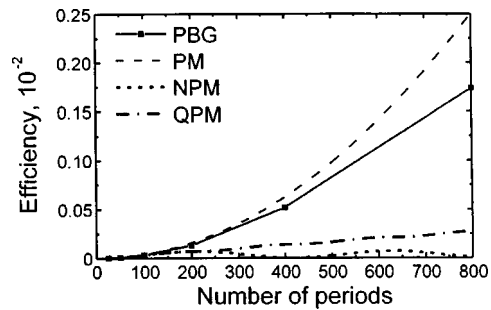


FIG. 3. Dependence of the efficiency of second-harmonic generation on the length of the nonlinear medium (expressed in periods of the photonic bandgap structure) for a photonic bandgap structure (solid curve), a structure designed for quasi-matched interaction (dot-dash curve), and a nonlinear medium with an uncompensated phase and group-velocity mismatch (dotted curve). The dashed curve represents a quadratic dependence on the length of the medium, corresponding to matched second-harmonic generation.

tures subject to the above-determined conditions can be used to satisfy the phase and group-velocity matching conditions simultaneously, the matched second-harmonic generation regime can be achieved for extremely short (a few periods of the light field) pulses using long photonic bandgap structures.

In summary, one-dimensional photonic bandgap structures provide a means for establishing not only phase matching conditions, but also group-velocity matching conditions for second-harmonic generation involving light pulses having a duration of a few periods of the optical field. When these conditions are satisfied, optical frequency doublers incorporating photonic bandgap structures can be used to increase the rate of growth of the second-harmonic signal as a function of the nonlinear-optical interaction length relative to structures utilizing quasi-matched interaction, and they offer capabilities for attaining high frequency doubling efficiencies independently of the matching length in the bulk nonlinear material.

These investigations are supported by the Constellation Group GmbH, the International Association for the Promotion of Cooperation with Scientists from the Independent States of the Former Soviet Union (INTAS Grant #97-0369), and the Moscow Government (Grant #A059).

¹S. A. Akhmanov and R. V. Khokhlov, *Problems in Nonlinear Optics* [in Russian], VINITI, Moscow (1964).

²N. Bloembergen, *Nonlinear Optics*, Benjamin, New York (1965).

³M. M. Fejer, G. A. Magel, D. H. Jundt, and R. L. Byer, *IEEE J. Quantum Electron.* **QE-28**, 2631 (1992).

⁴R. L. Byer, *J. Nonlinear Opt. Phys. Mater.* **6**, 549 (1997).

⁵J. A. Armstrong, N. Bloembergen, J. Ducuing, and P. S. Pershan, *Phys. Rev.* **127**, 1918 (1962).

⁶M. Scalora, M. J. Bloemer, A. S. Manka *et al.*, *Phys. Rev. A* **56**, 3166 (1997).

⁷M. Centini, C. Sibilina, M. Scalora *et al.*, *Phys. Rev. E* **60**, 4891 (1999).

⁸N. Bloembergen and A. J. Sievers, *Appl. Phys. Lett.* **17**, 483 (1970).

⁹P. Tran, *Opt. Lett.* **21**, 1138 (1996).

¹⁰N. I. Koroteev, S. A. Magnitskii, A. V. Tarasishin, and A. M. Zheltikov, *Opt. Commun.* **159**, 191 (1999).

¹¹A. Taflov, *Computational Electrodynamics: The Finite-Difference Time-Domain Method*, Artech House, Norwood, Mass. (1995).

Comment on the paper “Subwavelength diameter of light beams in active waveguides”

S. K. Sekatskii

Institute of Spectroscopy, Russian Academy of Sciences, 142092 Troitsk, Moscow Region, Russia

G. Dietler

Institut de Physique de la Matière Condensée, Université de Lausanne, CH-1015 Lausanne-Dorigny, Switzerland

(Submitted 25 October 1999)

Pis'ma Zh. Éksp. Teor. Fiz. **70**, No. 12, 806–807 (25 December 1999)

[S0021-3640(99)00824-5]

PACS numbers: 42.65.Wi, 42.25.Bs

In a recent paper¹ Kuznetsova considered the case of a cylindrical waveguide containing an amplifying medium and concluded that there is no frequency cutoff for such a case: for an arbitrary small radius a of the waveguide (but smaller than the cutoff radius a_{cut}) and an arbitrary small amplification δ (thus the complex permittivity of a medium is $\chi = \epsilon - i\delta$), light can propagate through such a waveguide with an amplification. This possibility, if it exists, of course, would be of extreme importance for near-field optics and fiber communications.

But it is not the case, because the analysis given in Ref. 1 is incorrect. The conclusions derived there are based on the use of the cylindrical wave equation to describe the electric field \mathbf{E} for the spherically symmetric TE mode (in this comment we follow the notation and concrete example given in Ref. 1; the analysis is similar for all waveguide modes):

$$\frac{\partial^2 E}{\partial z^2} + \frac{\partial}{\partial \rho} \left(\frac{1}{\rho} \frac{\partial}{\partial \rho} (\rho E) \right) + \epsilon \frac{\omega^2}{c^2} E = 0 \quad (1)$$

whose solution for the boundary condition

$$E(\rho = a, z) = 0 \quad (2)$$

for the case of a real permittivity is well known: $E = AJ_0(q\rho)\exp(pz)$. Here J_0 is the zero-order Bessel function, $q = 3.83/a$, and p can be found from the relation:

$$p^2 = q^2 - \epsilon \frac{\omega^2}{c^2}. \quad (3)$$

Kuznetsova generalized Eq. (3) to the case of a complex permittivity [and thus the complex coefficient p can be found as the square root of the right-hand side of (3)] and arrived at the aforementioned conclusions that a *propagating and amplified* wave exists for such a waveguide. This conclusion is wrong and results from the incorrect selection

of signs of the real and imaginary parts of the coefficient p , made on the unclear basis that “it is evident that ... the direction of growth of the wave is the same as the direction of propagation.”

This mistake can be easily understood from the following example. For the case when $a \ll a_{\text{cut}}$ and δ is arbitrarily small, Kuznetsova found that the amplification of the wave inside the waveguide is approximately equal to the q , i.e., the same as the damping for the case of small losses or an empty waveguide, and explained that this is due to the fact that “the wave propagates almost perpendicularly to the waveguide walls,” thus acquiring the necessary gain coefficient during this long path in an amplifying medium. But does that mean that the damping for the case of positive δ (losses) is also due to such a “perpendicular” propagation? And what does one do when there are no losses at all but the damping is the same?

Indeed, the correct selection of signs of the real and imaginary parts of the coefficient p is different from that given in Ref. 1. (This is especially clear if one directly substitutes the expression $E = AJ(\rho)\exp(p'z + ip''z)$ into (1) and then uses the theorem that Bessel functions of order greater than -1 have only real zeroes² to fulfill the boundary conditions (2). We will not do it here for lack of space). There is only one physically reasonable solution:

$$(p')^2 = \frac{1}{2} \left(\gamma^2 + \sqrt{\gamma^4 + \delta^2 \frac{\omega^4}{c^4}} \right), \quad p'' = \frac{\delta}{2p'} \frac{\omega^2}{c^2}$$

and the negative sign should be used when finding p' from the square root. (Here $\gamma^2 = q^2 - \epsilon(\omega^2/c^2)$ is the square of the damping constant for an empty waveguide (3), which is positive when $a < a_{\text{cut}}$.)

This solution describes an evanescent nonpropagating wave decreasing exponentially as $\exp(-|p'|z)$ for the case of a waveguide with radius smaller than the cutoff radius a_{cut} . Moreover, the rate of damping of this wave does not depend on the sign of δ and is larger for both amplifying and absorbing media in comparison with an empty waveguide. Indeed, this is not so surprising, because physically the cutoff phenomenon is nothing more than a *reflection* of the propagating wave from subwavelength apertures and is governed by the phase relations. The existence of an amplifying medium on the other side of the aperture cannot fundamentally alter the conditions of such a reflection. What it can do is to increase the reflectivity coefficient, which can be higher than unity, as happens, for example, in the case of total internal reflection of light from an amplifying medium:³ some amount of energy can be added to the reflected light for such a case. Thus, unfortunately, bright subwavelength-size sources of light cannot be produced by small subwavelength-aperture waveguides filled with an amplifying medium, and other ways to solve this fundamental problem for near-field optics must be found.

¹T. I. Kuznetsova, JETP Lett. **69**, 917 (1999).

²G. N. Watson, *A Treatise on the Theory of Bessel Functions*, Cambridge Univ. Press, Cambridge (1958), p. 482.

³F. Schuller, G. Niehnuis, and M. Ducloy, Phys. Rev. A **43**, 443 (1991).

Reply to the comment of S. K. Sekatskiĭ and G. Dietler

T. I. Kuznetsova*)

P. N. Lebedev Physics Institute, Russian Academy of Sciences, 117924 Moscow, Russia

(Submitted 25 November 1999)

Pis'ma Zh. Éksp. Teor. Fiz. **70**, No. 12, 808–809 (25 December 1999)

[S0021-3640(99)00924-X]

PACS numbers: 42.65.Wi, 42.25.Bs

In this note additional details and equations are furnished to support the validity of the conclusions drawn in Ref. 1.

1. A wave of the form $E = AJ_1(q\rho)\exp(pz)$ (see footnote¹) is discussed in Ref. 1. The waveguide is assumed to be circular and to have perfectly reflecting walls. The observed monochromatic field is characterized by the expression $\text{Re}\{E \exp(-i\omega t)\}$. With this choice of time factor and for $\delta > 0$ the dielectric permittivity $\varepsilon = 1 - i\delta$ implies amplification. The quantity p in the argument of the exponential is given by the equation

$$p \equiv p' + ip'' = \sqrt{q^2 - (\omega^2/c^2) + i\delta(\omega^2/c^2)}. \quad (1)$$

From this equation we can infer at once that p' and p'' have the same sign, because squaring both sides of Eq. (1) and then comparing the imaginary parts yields $2p'p'' = \delta(\omega^2/c^2)$. In an amplifying waveguide, therefore, the intensity increases in the direction of wave propagation.

We now give more detailed equations for p' and p'' . Denoting by a_{cr} the critical (at the frequency ω) waveguide radius, and by a the instantaneous radius, we set

$$q \frac{c}{\omega} \equiv \frac{q}{q_{\text{cr}}} = \frac{a_{\text{cr}}}{a}. \quad (2)$$

Using the transformation (2), we obtain the roots of the complex number (1) in the form

$$p'_{(1)} \frac{c}{\omega} = \sqrt{\sqrt{\frac{1}{4} \left(\frac{a_{\text{cr}}}{a}\right)^4 + \delta^2} + \frac{1}{2} \left(\frac{a_{\text{cr}}}{a}\right)^2}, \quad (3a)$$

$$p''_{(1)} \frac{c}{\omega} = (\text{sgn}(\delta)) \sqrt{\sqrt{\frac{1}{4} \left(\frac{a_{\text{cr}}}{a}\right)^4 + \delta^2} - \frac{1}{2} \left(\frac{a_{\text{cr}}}{a}\right)^2}, \quad (3b)$$

$$p'_{(2)} = -p'_{(1)}, \quad p''_{(2)} = -p''_{(1)}. \quad (4)$$

The arithmetic values of the roots are tacitly understood everywhere in Eqs. (3). The resulting solutions (3) and (4) are equally justified in every respect — contrary to what is stated in the comment — and there is no foundation for assigning preference to either over the other. These are the equations used to plot the graphs in the original article

showing the quantities $p'_{(1)}c/\omega$ and $p''_{(1)}c/\omega$ as functions of the dimensionless radius a/a_{cr} . For the sake of brevity the equations themselves are not given in the article. The graphs are given for the first solution [Eqs. (3)]. This choice was simply a matter of practicality in composing the figures. In the explanatory text relating to the figures it is stated that each of the quantities p' and p'' changes sign for the second solution.

The authors of the comment insist that the first solution [Eqs. (3)] must be rejected, leaving the second solution [Eq. (4)] as “the only physically reasonable” one. However, it is impossible to distinguish either solution so long as the symmetry of the problem is preserved. The substitution $z \rightarrow -z$ maps one solution into the other and maps the waveguide into itself. It is not so remarkable here that one of the waves grows along the z axis. The important consideration is that for each wave the growth of the intensity and the motion of the constant-phase surface take place in the same direction (p' and p'' have the same sign).

2. The comment touches casually on the coupling of the waveguide with free space. This problem is indeed important; for practical devices not only is wave transmission along the waveguide important, but so is wave reflection at the junctions of a finite segment of the waveguide with contiguous elements of the optical train. These considerations pose an independent problem and could not be combined with a different problem within the confines of a short publication. Techniques for matching a supercritical amplifying waveguide with other optical elements are currently under investigation. I should mention that the results of the investigation can affect only the input wave amplitudes in the waveguide, but not the growth rate and motion of the phase front, which are the topics treated in Ref. 1.

3. In regard to an absorbing waveguide it must be stated, contrary to the misgivings set forth in the comment, that here, as in an amplifying waveguide, the wavevector is almost perpendicular to the walls and has a small longitudinal component. To illustrate the matter, consider the electromagnetic energy flux associated with the wave. For the radiated TE_{01} mode it is equal to

$$S_z = \frac{c^2}{16\pi\omega} i \left(E \frac{\partial E^*}{\partial z} - E^* \frac{\partial E}{\partial z} \right). \quad (5)$$

Using the expression for E and Eq. (5), we find

$$S_z = \frac{c^2}{8\pi\omega} p'' |A|^2 [J_1(q\rho)]^2 \exp(2p'z). \quad (6)$$

It follows from Eq. (6) that for $p'' > 0$ the flux is positive, i.e., moves in the direction of increasing intensity (signs of p' and p''). These directions are the opposite in an absorbing medium. In both cases the flux is proportional to the small quantity p'' , which contains the small parameter δ . The flux becomes equal to zero for $\delta = 0$. The expression for the flux further emphasizes that the investigated waves propagate and grow in the direction of propagation in the amplification case (and decay in this direction in the absorption case). Therefore, the properties of the wave modes of an active waveguide have been derived and presented correctly.

*E-mail: tkuzn.@sci.lebedev.ru

¹Here J_1 is the first-order Bessel function. The function used in the comment is J_0 , which satisfies neither Eq. (1) in the comment nor Eq. (1) in Ref. 1.

¹T. I. Kuznetsova, JETP Lett. **69**, 917 (1999).

Translated by James S. Wood

IN MEMORY OF OUR AUTHORS

Pis'ma Zh. Éksp. Teor. Fiz. **70**, No. 12, 810 (25 December 1999)

[S0021-3640(99)01024-5]

PACS numbers: 01.60.+q, 78.55.Ap, 71.70.Ej

**V. F. MASTEROV, contributing author in this issue of the journal to the article
“Observation of fine structure in the photoluminescence spectrum of an Er³⁺ ion in an
amorphous silicon matrix”**

On January 28, 1999, Professor Vadim Fedorovich Masterov, Doctor of Physico-mathematical Sciences and Chairman of the Experimental Physics Department of St. Petersburg State Technical University, died unexpectedly at the age of 58. Prof. Masterov's experimental and theoretical papers on the electronic structure of deep multiple-electron centers in semiconductors and the high-temperature superconductivity of complex metal oxides of copper and metallic fullerenes have earned worldwide recognition. Prof. Masterov's scientific career has been permanently linked with preeminent science centers in Russia and in many foreign countries. He served as a member of organizing committees and program committees of many international and Russian conferences, as a member of the editorial board of the Journal *Fizika i Tekhnika Poluprovodnikov* (published in English as *Semiconductors*), and as a member of scientific councils of a great many state programs. Sixteen candidate's dissertations have been successfully defended under the sponsorship of V. F. Masterov, and four of his students have defended doctoral dissertations. The radiant memory of Vadim Fedorovich Masterov — an outstanding scientist and human being — will remain always with his innumerable students, colleagues, and friends.

**V. D. NEGRİİ, contributing author in this issue of the journal to the article “Photoinduced
transformation of luminescence centers in C₆₀ crystals at high pressure”**

On November 29, 1999, the gifted experimental physicist, Valeriĭ Dmitrievich Negriĭ, Chief Scientist of the Institute of Solid-State Physics of the Russian Academy of Sciences, died unexpectedly at the age of 60. He has published a vast number of papers on the optical spectroscopy of defects in semiconductors and dielectrics. His name is well known among scientists engaged in research on wide-gap II-VI semiconductors. One of his achievements in this field was the direct observation of photoluminescence of individual dislocations in CdS crystals and the investigation of distinctive characteristics of the motion and multiplication of dislocations in these crystals at low temperatures, including the laser stimulation of such processes. The most recent series of investigations reported by V. D. Negriĭ has been concerned with the photoluminescence of fullerene crystals — a new and intriguing class of organic semiconductors, where he discovered many interesting phenomena associated with photostimulated reactions of defects in these crystals.